Glassy dynamics and dynamical heterogeneity in colloids

Luca Cipelletti

LCVN, UMR 5587 Université Montpellier 2 and CNRS, P. Bataillon 34095 Montpellier, France.

Eric R. Weeks

Department of Physics,Emory University; Mail stop 1131/002/1AB 400 Dowman Dr. Atlanta GA 30322-2430 USA.

OXFORD
UNIVERSITY PRESS

Abstract

Concentrated colloidal suspensions are a well-tested model system which has a glass transition. Colloids are suspensions of small solid particles in a liquid, and exhibit glassy behavior when the particle concentration is high; the particles are roughly analogous to individual molecules in a traditional glass. Because the particle size can be large (100 nm - 1000 nm), these samples can be studied with a variety of optical techniques including microscopy and dynamic light scattering. Here we review the phenomena associated with the colloidal glass transition, and in particular discuss observations of spatial and temporally heterogeneous dynamics within colloidal samples near the glass transition. Although this Chapter focuses primarily on results from hard-sphere-like colloidal particles, we also discuss other colloidal systems with attractive or soft repulsive interactions.

0.1 Colloidal hard spheres as a model system for the glass transition

0.1.1 The hard sphere colloidal glass transition

When some materials are rapidly cooled, they form an amorphous solid known as a glass. This transition to a disordered solid is the glass transition (Götze and Sjogren, 1992; Stillinger, 1995; Ediger *et al.*, 1996; Angell *et al.*, 2000). As the temperature of a molecular glass-forming material is decreased the viscosity rises smoothly but rapidly, with little apparent change in the microscopic structure (Ernst *et al.*, 1991; van Blaaderen and Wiltzius, 1995). Glass formation may result from dense regions of well-packed molecules or a decreasing probability of finding mobile regions. As no structural mechanisms for this transition have been found, many explanations rely on dynamic mechanisms. Some theoretical explanations focus on the idea of dynamical heterogeneities (Götze and Sjogren, 1992; Sillescu, 1999; Ediger, 2000; Adam and Gibbs, 1965). The underlying concept is that, for any molecule to move, all molecules within a surrounding region must "cooperate" in their movement. As the glass transition is approached the sizes of these regions grow, causing the rise in macroscopic viscosity (Adam and Gibbs, 1965). The microscopic length scale characterizing the size of these regions could potentially diverge, helping explain the macroscopic viscosity divergence. However, it is also possible that these regions could grow but not be directly connected to the viscosity divergence. Additionally, it is not completely clear if the viscosity itself diverges or simply becomes too large to measure (Hecksher *et al.*, 2008). While the existence of dynamical heterogeneities in glassy systems has been confirmed in a wide variety of systems, the details of this conceptual picture remain in debate (Sillescu, 1999; Ediger, 2000; Glotzer, 2000; Ngai, 1999; Richert, 2002; Cipelletti and Ramos, 2005).

Colloidal suspensions are composed of microscopic-sized solid particles in a liquid, and are a useful model system for studying the glass transition. In terms of interparticle

interaction, the simplest colloids are those in which the particles interact as hard spheres, i.e., the interparticle potential arises solely due to excluded volume effects (Pusey and van Megen, 1986). Hard spheres are a useful theoretical model for glass-forming systems due to their simplicity (Bernal, 1964). Clearly, attractive interactions between atoms and molecules are responsible for dense phases of matter. But given dense states of matter, repulsive interactions play the dominant role in determining the structure. Hard spheres are useful simulation models for crystals, liquids, and glasses, although it is still debated whether a purely repulsive interparticle potential is sufficient to reproduce the glass transition in general (Berthier and Tarjus, 2009).

The control parameter for hard sphere systems is the concentration, expressed as the fraction, φ, of the sample volume occupied by the particles. Most colloidal hard sphere systems act like a glass for φ larger than an "operational" glass transition volume fraction $\varphi_g \approx 0.58$. The transition is the point where particles no longer diffuse through the sample on experimentally accessible time scales; for $\varphi < \varphi_g$ spheres do diffuse at long times, although the asymptotic diffusion coefficient D_∞ decreases sharply as the concentration increases (Bartsch *et al.*, 1993; van Megen *et al.*, 1998; Kasper *et al.*, 1998). The transition at φ_g occurs even though the spheres are not completely packed together; in fact, the density must be increased to $\varphi_{\mathrm{RCP}} \approx 0.64$ for "random-close-packed" spheres (O'Hern *et al.*, 2003; Bernal, 1964; Torquato *et al.*, 2000; Donev *et al.*, 2004; O'Hern *et al.*, 2004) before the spheres are motionless. In simulations, a collection of same-sized (i.e. monodisperse) hard spheres almost always crystallizes. A binary mixture of spheres or indeed a distribution of sizes is therefore needed to frustrate crystallization and enable access to the glass transition, both numerically and experimentally (Henderson and van Megen, 1998; Zaccarelli *et al.*, 2009*a*).

The glass transition for suspensions of nearly-hard-sphere colloids (Pusey and van Megen, 1986; van Megen and Pusey, 1991; van Blaaderen and Wiltzius, 1995; van Megen and Underwood, 1993; Bartsch *et al.*, 1993; Bartsch, 1995; Mason and Weitz, 1995) is comparable in many respects to the hard sphere glass transition studied in simulations and theory (Speedy, 1998). Macroscopically, a colloidal liquid flows like a viscous fluid whereas the colloidal glass does not flow easily, like a paste (Segrè *et al.*, 1995*b*; Cheng *et al.*, 2002). For colloidal samples with low polydispersity, samples can crystallize for $\varphi < \varphi_g$ (with crystallization nucleating in the interior of the sample), while for $\varphi > \varphi_g$, crystals only nucleate at flat sample boundaries such as the walls of the container (Pusey and van Megen, 1986). Microscopically, the glass transition point is identified as the point where $D_\infty \to 0$ (Bartsch *et al.*, 1993; van Megen *et al.*, 1998; Kasper *et al.*, 1998).

Note that there are some questions about the colloidal glass transition. First, prior measurements disagree about the nature of the viscosity divergence in colloidal glasses (Segrè *et al.*, 1995*b*; Cheng *et al.*, 2002). This may be due to difficulties in reconciling measurements of the volume fraction φ (de Schepper *et al.*, 1996; Segrè *et al.*, 1996). Second, it has been seen that a glassy colloidal suspension can crystallize under microgravity conditions (Zhu *et al.*, 1997), and potentially also when in density-matching solvents (Kegel, 2000; Simeonova and Kegel, 2004), suggesting that the apparent glass transition at $\varphi_g = 0.58$ is an artifact of gravity. The interpretation of these observations is unclear. One possibility is that this is merely heterogeneous nucleation at the walls, as seen before (Pusey and van Megen, 1986). Another possi-

bility is that these samples were more monodisperse than most, and a slightly larger polydispersity ($> 5\%$) may be necessary to induce a glass transition at $\varphi_g = 0.58$ (Henderson and van Megen, 1998; Meller and Stavans, 1992; Auer and Frenkel, 2001; Schope *et al.*, 2007). In practice, most experimental samples always have a polydispersity of at least 5%. Recent simulations suggest that the relationship between polydispersity, crystallization, and glassy dynamics is more complex than perhaps was previously appreciated (Zaccarelli *et al.*, 2009*a*). Overall we note that the interpretations of the various observations described in this paragraph are often still controversial.

Colloidal glasses are quite similar to molecular glasses:

- Both are microscopically disordered (van Blaaderen and Wiltzius, 1995).
- Both are macroscopically extremely viscous near their transition point (Segrè *et al.*, 1995*b*; Cheng *et al.*, 2002).
- Colloidal glasses have a nonzero elastic modulus at zero frequency, which is absent in the liquid phase (Mason and Weitz, 1995).
- Colloidal glasses are out of equilibrium and show aging behavior – their properties depend on the time elapsed since preparation (Courtland and Weeks, 2003; Cianci *et al.*, 2006; Cianci and Weeks, 2007; Simeonova and Kegel, 2004), similar to polymer glasses (Hodge, 1995; McKenna, 2003) and other molecular glasses (Angell *et al.*, 2000; Castillo and Parsaeian, 2007).
- Colloidal glasses exhibit dynamical heterogeneity (Kegel and van Blaaderen, 2000; Weeks *et al.*, 2000), similar to that seen in simulations (Donati *et al.*, 1998; Glotzer, 2000; Doliwa and Heuer, 1998) and experiments on molecular glasses (Ediger, 2000; Sillescu, 1999; Vidal Russell and Israeloff, 2000).
- The colloidal glass transition is sensitive to finite size effects (Nugent *et al.*, 2007), similar to molecular glasses (Alcoutlabi and McKenna, 2005) and polymers (Roth and Dutcher, 2005).

One difference between colloids and molecules is that colloidal particles move via Brownian motion whereas the latter move ballistically at very short time scales; several simulations indicate that this difference is unimportant for the long-time dynamics which is of the most interest (Gleim *et al.*, 1998; Szamel and Flenner, 2004; Höfling *et al.*, 2008). Likewise, hydrodynamic interactions between particles influence their motion on short time scales, but do not modify the pairwise interaction potential (which remains hard-sphere-like), suggesting that they should not be relevant for the long-time dynamics (Brambilla *et al.*, 2009).

One advantage colloids have over traditional molecular glassformers is that their time scales are significantly slower, with relaxation taking O(1-1000 s), allowing easy study of the relaxation processes. A second advantage of colloids is that their large size [$O(1\ \mu\text{m})$] allows for measurement using optical microscopy or dynamic light scattering, as will be discussed in Sec. 0.2.

Experiments have one chief advantage over simulations, in that they more easily avoid finite size effects. Near the glass transition, dynamical length scales can be large ($\sim 4-5$ particle diameters (Weeks *et al.*, 2007; Doliwa and Heuer, 2000)) and finite size effects on structure and dynamics may extend to even larger length scales (~ 20 particle diameters (Nugent *et al.*, 2007)). Microscope sample chambers typically contain $\sim 10^9$ particles, and light scattering cuvettes contain even more.

The most popular "hard sphere" colloid is colloidal PMMA (poly-methyl-methacrylate),

sterically stabilized to minimize inter-particle attraction (Pusey and van Megen, 1986; Weeks *et al.*, 2000; Dinsmore *et al.*, 2001; Antl *et al.*, 1986). The particles can be placed in density-matching solvents to inhibit sedimentation (see Sec. 0.1.2), and/or solvents which match their index of refraction to enable microscopy (Dinsmore *et al.*, 2001) and light scattering (see Secs. 0.2.2 and 0.2.3). In some of these solvents, the particles pick up a slight charge and thus have a slightly soft repulsive interaction in addition to the hard-sphere core. Despite this charge the spheres behave similarly to hard spheres with some phase transitions shifted to slightly lower φ (Gasser *et al.*, 2001). Salt can be added to the samples to screen the charges and shift the interaction back to more hard-sphere like (Yethiraj and van Blaaderen, 2003; Royall *et al.*, 2003).

A second popular colloid is colloidal silica, which is relatively easy to fabricate (Stober, 1968). These particles are suspended in water (or a mixture of water and glycerol), avoiding the organic solvents that are required for PMMA colloids. Because they are in water, repulsion due to charge is the primary mechanism preventing flocculation; adding salt can screen the charges and cause flocculation (which is often irreversible). Silica colloids are hard to density match (their density varies but is larger than 2 g/cm^3), and also it is hard to match their refractive index. This latter constraint makes microscopy difficult except at lower volume fractions (Mohraz *et al.*, 2008).

Several glass transition theories have been applied to the colloidal glass transition. The colloidal glass transition appears to be well-described by mode-coupling theory up to $\varphi \approx 0.58$ (van Megen and Pusey, 1991; van Megen and Underwood, 1993; van Megen and Underwood, 1994; Götze and Sjögren, 1991; Schweizer and Saltzman, 2003; Schweizer and Saltzman, 2004; Saltzman and Schweizer, 2006*b*; Saltzman and Schweizer, 2006*a*), although other glass transition theories successfully capture many features of the colloidal glass transition as well (Ngai and Rendell, 1998; Liu and Oppenheim, 1996; Tokuyama and Oppenheim, 1995; Tokuyama, 2007). (See the discussion in Sec. 0.3.1 which discusses the strengths and weaknesses of mode-coupling theory as applied to colloids.)

0.1.2 Experimental challenges in studying colloidal hard spheres

As argued in the previous section, colloidal hard spheres are a good model system for investigating the glass transition. However, several experimental challenges have to be faced. Probably, the most serious problem is that of a precise determination of the volume fraction. In optical microscopy, φ can be obtained by counting the number of particles in a given volume and using the particle size as obtained, e.g., from electron microscopy. It should be noted that an error of just 1% in the radius a of the particles results in a 3% error in φ. Additionally, one has to take into account the thickness of the stabilizing layer (e.g. the grafted polymer for PMMA particles or the counterion cloud for silica particles in a polar solvent), which is often difficult to measure precisely. Since typical values of the thickness are on the order of 10 nm (Pusey, 1991), this contribution can be relevant for the small particles used in light scattering ($a \sim 100 - 300$ nm), while it is less important for the micron-sized particles used in microscopy. Other methods to determine φ include precise density or refractive index measurements (Phan *et al.*, 1996). For PMMA, these methods require special care, since the particles can be swollen by organic solvents such as tetralin or

brominated solvents, which change their density and refractive index compared to those of the bulk material.

Because of these difficulties, the absolute volume fraction is often determined indirectly by comparing the phase behavior or the dynamical behavior of the sample to theoretical and numerical predictions. Samples sufficiently monodisperse ($\sigma = \sqrt{\overline{a^2} - \overline{a}^2}/\overline{a}^2 < 5-8\%$) crystallize for $0.494 < \varphi < 0.545$ (Pusey, 1991). The absolute volume fraction can then be calibrated by matching the experimentally determined freezing volume fraction with $\varphi_f = 0.494$ as determined by simulations (Hoover and Ree, 1968). However, some uncertainty is still left, because the exact value of the freezing fraction depends on σ (Bolhuis and Kofke, 1996; Fasolo and Sollich, 2004; van Megen and Underwood, 1994; Zaccarelli *et al.*, 2009*a*; Pusey *et al.*, 2009). Moreover, this method cannot be applied to more polydisperse suspensions that do not crystallize over several months or years. Alternatively, φ may be calibrated against predictions for the volume fraction dependence of the low shear viscosity (Pusey, 1991; Poon *et al.*, 1996) or the short time self diffusion coefficient (Beenakker and Mazur, 1983; Tokuyama and Oppenheim, 1994) in the dilute regime. For samples where both the calibration against φ_f and that using the short time self diffusion coefficient are possible, the two methods appear to be consistent (van Megen and Underwood, 1989; Segrè *et al.*, 1995*a*). In summary, while relative values of φ can be measured very precisely (down to 10^{-4} using an analytical balance), absolute values are typically affected by an uncertainty of a few %. This should always be kept in mind when comparing sets of data obtained in different experiments.

For colloids, the equivalent of $T = 0$ in a molecular system is random close packing, the volume fraction $\varphi_{\mathrm{RCP}} \sim 0.64$ where osmotic pressure diverges and all motion ceases because no free volume is left. Clearly, knowledge of the precise location of φ_{RCP} is very important to discriminate between theories that predict a glass transition below random close packing (for example the mode coupling theory (Gotze, 1999) or thermodynamic glass transition theories (Cardenas *et al.*, 1999; Parisi and Zamponi, 2005)) and scenarios like jamming, where no arrest is predicted below φ_{RCP}. However, the location of random close packing is still highly debated (Berthier and Witten, 2009; Xu *et al.*, 2009; Kamien and Liu, 2007; Chaudhuri *et al.*, 2010) and its very existence is challenged, based on the argument that one can always trade order for packing efficiency (Donev *et al.*, 2007), up to $\varphi = \pi/\sqrt{18} \approx 0.7405$, the packing fraction of a (monodisperse) hard sphere crystal. Experimentally, it is difficult to measure φ_{RCP} because of the uncertainty on absolute volume fractions discussed above and because applying the high pressure (e.g. by centrifugation) needed to approach it may result in the compression of the stabilizing layer. Additionally, both experiments (Clusel *et al.*, 2009) and simulations (Schaertl and Sillescu, 1994; Berthier and Witten, 2009) show that φ_{RCP} depends on σ.

Some of the experimental challenges posed by hard spheres stem from the very same features that make them a valuable model system: their relatively large time and length scales. The microscopic time in a colloidal system is the Brownian time τ_B, i.e. the time required by a particle to diffuse over its own size in a diluted system, defined as

$$\tau_B \equiv a^2/6D = \pi\eta a^3/k_B T\,. \tag{0.1}$$

Here, η is the solvent viscosity, T the absolute temperature, k_B Boltzman's constant and D is the diffusion coefficient for a sphere of radius a, given by the Stokes-Einstein-Sutherland formula (Einstein, 1905; Sutherland, 1905):

$$D = k_B T / 6\pi\eta a \,. \tag{0.2}$$

The time scale τ_B is typically on the order of $10^{-3} - 1$ s. The largest relaxation time that can be measured in concentrated systems is on the order of 10^5 s; thus, the accessible dynamical range covers at most 8 decades, as opposed to 15 decades in molecular glass formers. Additionally, owing to their relatively large size and due to the mismatch between their density and that of the solvent in which they are suspended, colloidal particles experience gravitational forces that can modify their phase behavior (Zhu *et al.*, 1997; Pusey *et al.*, 2009) and dynamical properties (El Masri *et al.*, 2009; Simeonova and Kegel, 2004). The relevant parameter to gauge the importance of sedimentation is the inverse Péclet number, $Pe^{-1} = \frac{3k_B T}{4\Delta\rho g a^4}$, defined as the ratio of the gravitational length to the particle radius (g is the acceleration of gravity and $\Delta\rho$ the density mismatch). For diluted suspensions, gravity becomes relevant as Pe^{-1} approaches (from above) unity; for concentrated suspensions, sedimentation effects may set in at even higher values of Pe^{-1}, since gravitational stress is transmitted over increasingly larger distances as the sample becomes more solid-like. For example, sedimentation effects have been reported to alter the dynamics of PMMA particles in organic solvents ($\Delta\rho \sim 0.3\mathrm{g/cm}^3$) for $Pe^{-1} = 44.1$ (Simeonova and Kegel, 2004) or even for $Pe^{-1} = 1350$ (El Masri *et al.*, 2009). Density- matching solvents can mitigate these effects, although matching closely both the index of refraction (as required for optical observations) and the density of the particles without altering their hard sphere behavior has been proved difficult for PMMA particles (Royall *et al.*, 2003) and impossible for other systems such as silica spheres.

0.2 Experimental methods for measuring both the average dynamics and dynamical heterogeneity

0.2.1 Main features of optical microscopy and dynamic light scattering

Optical microscopy and dynamic light scattering are the main techniques to probe both the average dynamics and its spatiotemporal fluctuations in dense colloidal suspensions. Each of them comes with specific advantages and limitations. Optical microscopy is unsurpassed in providing detailed information on the structure and the dynamics at the single particle level. The same quantities introduced in theory and simulations to characterize the dynamics can be precisely measured (e.g. the mean square displacement or the intermediate scattering function for the average dynamics, and the dynamical susceptibility, χ_4, and the spatial correlation of the dynamics, g_4, for its fluctuations, see Chapter 2 and Sec. 0.2.4 below). Additionally, direct visualization of the sample allows any experimental problem to be readily detected, such as particle aggregation, sedimentation, or wall effects. Finally, techniques such as optical or magnetic tweezing (Grier, 2003; Amblard *et al.*, 1996) allow one to manipulate single particles and thus to measure the microscopic response of the system to a local perturbation (Habdas *et al.*, 2004).

Dynamic light scattering probes a very large number of particles simultaneously, yielding very good averages. Moreover, particles used in light scattering are usually smaller than those for optical microscopy ($a = 100 - 500$ nm as opposed to $a = 0.5 - 1.5\mu$m), which has a twofold advantage. First, the microscopic time τ_B (see Eq. (0.1)) is significantly reduced, since $\tau_B \sim a^2/D \sim a^3$, thus increasing substantially the experimentally accessible dynamical range. Second, gravitational effects are much less of concern, since $Pe^{-1} \sim a^{-4}$. Finally, as we will discuss it in Sec. 0.2.4, recent developments allow dynamical heterogeneity to be probed by dynamic light scattering, although not at the level of microscopic detail afforded by optical microscopy. These methods extend the possibilities of light scattering by adding features characteristic of imaging techniques. Quite in a symmetric way, very recent microscopy methods such as dynamic differential microscopy (Cerbino and Trappe, 2008) have extended imaging techniques by adding the capability of measuring the intermediate scattering function $f(q, \tau)$ defined below in Sec. 0.2.3.

0.2.2 Optical and confocal microscopy

Given the large size of many colloidal systems (particle radius $a \sim 100 - 1000$ nm), optical microscopy is a useful tool for observing these systems. First, these sizes are comparable to the wavelength of light, thus rendering them visible. Second, the time scales of their motion are often slow enough for video cameras to follow their motion. This can be seen by considering how quickly particles diffuse. Colloidal particles undergo Brownian motion due to thermal fluctuations, as discussed in Sec. 0.1.2. The diffusion coefficent D (Eq. 0.2) is related to the mean square displacement of particles as:

$$\langle \Delta x^2 \rangle = 2D\Delta t, \tag{0.3}$$

where Δt is the time scale over which the displacements are taken. A particle of diameter $2a = 1$ μm in water ($\eta = 1$ mPa·s) at room temperature diffuses approximately 1 μm in 1 s. This motion is easy to study with a conventional video camera and a microscope; most video cameras take data at 30 images per second, thus they allow one to follow the Brownian motion of colloidal particles of these sizes. Of course, particles that are 10 times smaller move 1000 times faster, by Eq. (0.1). In practice, often one can choose to study larger colloidal particles (Weeks *et al.*, 2000) or use careful data analysis techniques to learn information about smaller-sized particles that aren't directly imaged (Simeonova and Kegel, 2004). Additionally, when studying dense colloidal samples, the time scales increase simply because of the glassy dynamics.

Two main methods of microscopy have been used to study dense colloidal samples: conventional optical microscopy and confocal microscopy. First, there is the possibility of using a conventional light microscope technique such as "brightfield microscopy." These techniques typically depend on slight differences between the index of refraction of the colloidal particles and the solvent (Inoué and Spring, 1997). A limitation is that these differences also scatter light; each particle acts like a tiny lens. This ultimately limits how deeply into a sample one can observe. (This is the same phenomenon that makes milk appear white, even though composed of transparent components; the different components all have different indices of refraction. Snow is white for a similar reason, due to the contrast in index of refraction between the ice crystals

and air.) A further limitation of conventional optical microscopy is that the images are limited to a plane, although this can be fine for quasi-two-dimensional samples (Marcus *et al.*, 1999).

A related conventional technique is fluorescence microscopy. Here, the particles can be precisely index-matched with the solvent. However, the particles also contain a fluorescent dye. In fluorescence microscopy, the particles are illuminated with short-wavelength light. The dye molecules absorb this light, and radiate slightly longer wavelength (lower energy) light, which is imaged by the camera. Special filters and mirrors are used to direct the light appropriately from the light source to the sample, and from the sample to the camera. While this method avoids the problem of light scattering off of different parts of the sample, in dense samples it can still be a problem that too much of the sample fluoresces at the same time, thus giving a large background illumination. Trying to observe bright particles on a bright background thus limits fluorescence microscopy of dense samples. One way to overcome this is to only dye a few tracer particles.

Fluorescence microscopy has one significant limitation: photobleaching. After dye molecules absorb the excitation light, but before they emit light, they can chemically react with oxygen present in the sample to form a non-fluorescent molecule. This only happens when they are excited, so photobleaching happens in direct proportion to the illumination light. Photobleaching manifests itself as the image becoming gradually darker. This can be a useful technique for studying local diffusion in samples, a technique known as "fluorescent recovery after photobleaching" (Axelrod *et al.*, 1976). Intense light is used to photobleach a region of the sample, and then low-intensity light is used to monitor the recovery of fluorescence as non-bleached particles diffuse back into the region. With this method, the diffusivity of the particles can be measured, which has been used to study the behavior of colloidal glasses (Simeonova and Kegel, 2004).

An extension of fluorescence microscopy is confocal microscopy, sometimes termed laser scanning optical microscopy. Here, a laser is used to excite fluorescence in dye added to a sample. Typically, the laser beam is reflected off two scanning mirrors that raster the beam in the x and y directions on the sample. Any resulting fluorescent light is sent back through the microscope, and becomes descanned by the same mirrors. A mirror directs the fluorescent light onto a detector, usually a photomultiplier tube.

One additional modification is necessary to make a confocal microscope: before reaching the detector, the fluorescent light is focused onto a screen with a pinhole. All of the light from the focal point of the microscope passes through the pinhole, while any out of focus fluorescent light is blocked by this screen. This spatial filtering technique blocks out the background fluorescence light, allowing the particles to be viewed as bright objects on a dim background.

This ability to reject out-of-focus fluorescent light directly results in the main strength of confocal microscopy, the ability to take three-dimensional pictures of samples. By rejecting out-of-focus light, a crisp two-dimensional image can be obtained, as shown in Figure 0.1. The sample (or objective lens) can be moved so as to focus at a different height z within the sample, and a new 2D image obtained. By collecting a stack of 2D images at different heights z, a 3D image is built up. The time to scan one 2D image can range from 10 ms to several seconds, depending on the

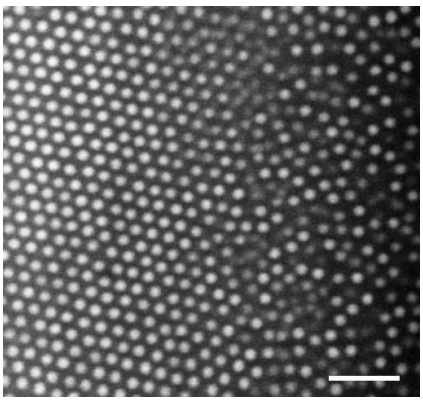

Fig. 0.1 Image of 2 micron diameter colloidal particles taken with a confocal microscope. The scale bar is 10 microns. The sample is in coexistence between a colloidal crystal and a liquid, see Ref. (Hernández-Guzmán and Weeks, 2009) for details. Taken by Jessica Hernández-Guzmán and Eric R. Weeks

details of the confocal microscope and the desired image size and quality. The time to scan a 3D image depends on the 2D scan speed and the desired number of pixels in the z-direction; reasonable 3D images can be acquired in 2 - 20 s depending on the microscope (Nugent *et al.*, 2007; Weeks *et al.*, 2000). Finally, we mention Coherent anti-Stokes Raman scattering (CARS) microscopy (Kaufman and Weitz, 2006), a technique that allows one to image in 3D colloidal samples with spatial and temporal resolutions comparable to those of confocal microscopy.

Once a series of images has been acquired (2D or 3D), the next step is typically tracking the individual particles within the images. Within each image, a computer can determine the positions of all of the particles. If the particles do not move large distances between subsequent images, then they can be easily tracked (Crocker and Grier, 1996). Specifically, they need to move less between images than their typical inter-particle spacing. With confocal microscopy, particles can be tracked in three dimensions (Besseling *et al.*, 2009; Dinsmore *et al.*, 2001). This then is the same type of data that is analyzed from computer simulations. Simulations, of course, have many advantages, including a tunability of particle interaction, the ability to study either Brownian or ballistic dynamics, and more precise and instantaneous control over parameters such as temperature and pressure. The experiments have an advantage that typically the boundaries are far away: while perhaps a few thousand particles might be viewed, they are embedded in a much larger sample with millions of particles.

0.2.3 Dynamic light scattering

Dynamic light scattering (DLS) (Berne and Pecora, 1976), also termed photon correlation spectroscopy, probes the temporal fluctuations of the refractive index of a sample. In colloidal systems, scattering arises from a mismatch between the index of refraction of particles and that of the solvent, so that DLS probes particle density fluc-

tuations. Experimentally, one measures $g_2(\tau)-1$, the time autocorrelation function of the temporal fluctuations of the intensity scattered at a wave vector $q = 4\pi/\lambda \sin(\theta/2)$. Here, θ is the scattering angle and λ is the wavelength in the solvent of the incoming light, usually a laser beam. Under single scattering conditions, the intensity autocorrelation function is directly related to the intermediate scattering function $f(q,\tau)$ (ISF, sometimes also referred to as the dynamic structure factor) :

$$f(q,\tau) \equiv \left\langle N^{-1} \sum_{j,k} \exp\left\{-i\mathbf{q}\cdot[\mathbf{r}_j(t+\tau)-\mathbf{r}_k(t)]\right\} \right\rangle$$
$$= \sqrt{\beta^{-1}[g_2(\tau)-1]} = \sqrt{\beta^{-1}\left[\frac{< I(t+\tau)I(t) >_t}{< I(t) >_t^2} - 1\right]}, \tag{0.4}$$

where $\beta \leq 1$ depends on the collection optics, $I(t)$ is the time varying scattered intensity, $\mathbf{r}_j$ the position of the j-th particle, and N the number of particles in the scattering volume. Note that $f(q,\tau)$ decays significantly when $\Delta\mathbf{r}(\tau) = \mathbf{r}(t+\tau)-\mathbf{r}(t)$ is of the order of q^{-1}: depending on the choice of θ, DLS probes motion on length scales ranging from tens of nm to tens of μm. Another important point to be noticed is that DLS usually probes collective motion, since the sum in Eq. (0.4) extends over all pairs of particles. However, there are ways to measure the self part of the ISF by making the contribution of the $j \neq k$ terms vanish from Eq. (0.4). This may be accomplished by choosing the scattering vector q in such a way that $S(q) = 1$, where $S(q)$ is the static structure factor (Pusey *et al.*, 1982; Pusey, 1978). Alternatively, one can use optically polydisperse suspensions, as in Ref. (van Megen and Underwood, 1989), where silica and PMMA particles of nearly the same radius but different refractive index were mixed. When matching the average refractive index of the colloids, the measured ISF contains only contributions from the self terms, $i = k$. Note that optically composite particles that are polydisperse in size are usually also optically polydisperse. This is the case, e.g., of PMMA colloids stabilized by polymer layer with a refractive index different from that of the core, when the core is polydisperse in size.

The nature of the averages indicated by the brackets in Eq. (0.4) is an important issue. In the definition of the ISF, the average is over an ensemble of statistically equivalent particle configurations, while operationally g_2 is averaged over time. Therefore, ergodicity is required for Eq. (0.4) to hold. Additionally, in order to reduce noise to an acceptable level, g_2 has to be averaged over at least $10^3-10^4\ \tau_\alpha$, with τ_α the relaxation time of the ISF. These requirements are often impossible to meet for supercooled or glassy colloidal systems, where τ_α can be as large as hundreds of thousands of seconds. To overcome these difficulties, various schemes have been proposed, among which the most popular is probably the "multispeckle" method (Wong and Wiltzius, 1993; Bartsch *et al.*, 1997). In a multispeckle experiment, the phototube or avalanche photodiode used in regular DLS is replaced by a multielement detector, typically a CCD or CMOS camera sensor. The collection optics is chosen in such a way that each pixel of the detector corresponds to a different speckle (Goodman, 2007), i.e. to a slightly different scattering vector. Because distinct speckles carry statistically independent information, the time average can be replaced in part by an average over pixels:

$$g_2(\tau) - 1 = \left\langle \frac{< I_p(t+\tau) I_p(t) >_p}{< I_p(t+\tau) >_p < I_p(t) >_p} - 1 \right\rangle_t . \tag{0.5}$$

Here I_p indicates the intensity measured by the $p-th$ pixel, $< \cdots >_t$ and $< \cdots >_p$ denote averages over time and pixels, respectively. The set of pixels is chosen in such a way that they correspond to nearly the same magnitude of the scattering vector q. The number of pixels is typically of order $10^4 - 10^5$, so that time averaging only needs to extend over a few τ_α. This approach allows very slow and non-stationary dynamics to be probed effectively.

Although many DLS experiments have been carried on a variety of glassy colloidal systems, the single-scattering conditions required by this technique are probably more the exception than the rule. For mildly turbid suspensions, smart detection schemes, most of which were pioneered by K. Schätzel (Schätzel, 1991), allow the rejection of multiply scattered photons, thereby efficiently suppressing artifacts due to multiple scattering. Popular implementations of this concept include the so-called two-color and 3-D apparatuses (see Ref. (Pusey, 1999) for a review). For very turbid samples, where photons are scattered a large number of times before leaving the sample and the contribution of single scattering is negligible, an alternative formalism has been developed, termed Diffusing Wave Spectroscopy (DWS) (Weitz and Pine, 1993). In a DWS experiment the intensity correlation function $g_2 - 1$ is related to the mean squared displacement, $< \Delta r^2(\tau) >$, rather than to the ISF, as in DLS. Another important difference is the probed length scale, which in DWS typically covers the range 0.1 - 100 nm, much smaller than in DLS. Finally, DWS experiments typically probe the self motion of the particles, rather than their collective relaxation.

An alternative way to tackle multiple scattering is provided by X-photon correlation spectroscopy (XPCS). Modern synchrotron sources deliver X-ray radiation that is coherent enough to perform the same kind of experiments as with a laser beam in DLS. Because colloidal systems scatter X-ray much less efficiently than visible light, in most cases XPCS measurements can be safely performed in the single scattering regime without adjusting the refractive index of the solvent. While long-term beam stability is often still an issue, several XPCS studies on the slow dynamics of colloidal systems have been published in the last years (Bandyopadhyay *et al.*, 2004; Chung *et al.*, 2006; Robert *et al.*, 2006; Trappe *et al.*, 2007; Wandersman *et al.*, 2008; Herzig *et al.*, 2009; Duri *et al.*, 2009*a*).

0.2.4 Time and space resolved dynamic light scattering

In a traditional DLS experiment, the detector is placed in the far field, so that it collects light scattered by a macroscopic region, typically of volume 1 mm^3 or more. Additionally, the intensity correlation function $g_2 - 1$ has to be extensively averaged over time. Because of these averages over both time and space, no information can be a priori extracted on dynamical heterogeneity, e.g. on the spatial and temporal fluctuations of the dynamics. In recent years, however, novel light scattering methods have been proposed to overcome these limitations, providing either spatially averaged but temporally resolved data (time resolved correlation, TRC (Cipelletti *et al.*, 2003)), or both spatially and temporally resolved measurements (photon correlation imaging, PCI (Duri *et al.*, 2009*b*)).

In a TRC experiment, one uses a CCD or CMOS detector to calculate a two-time correlation function $c_I(t,\tau)$ defined by

$$c_I(t,\tau) = \frac{< I_p(t+\tau) I_p(t) >_p}{< I_p(t+\tau) >_p < I_p(t) >_p} - 1\,. \tag{0.6}$$

Note that the usual intensity correlation function $g_2(\tau) - 1$ defined in Eq. (0.5) is the temporal average of $c_I(t,\tau)$. Because the detector is typically placed in the far field, c_I is a temporally resolved but spatially averaged correlation function. Figure 0.2 shows an example of TRC data and their relationship to $g_2 - 1$ for a diluted Brownian suspension (Duri *et al.*, 2005) and for a colloidal gel (Duri and Cipelletti, 2006). When plotted as a function of time t for a fixed time delay τ, the data for the Brownian suspension are essentially constant. Indeed, for this system the dynamics are homogeneous and time-translational invariant, so that the evolution of the system and hence the degree of correlation over a fixed time lag τ does not depend on t. The small fluctuations around the mean value are due to the statistical noise of the measurement, associated with the finite number of pixels over which c_I is averaged (Duri *et al.*, 2005). For the colloidal gel, by contrast, c_I exhibits significant temporal fluctuations, indicative of heterogeneous dynamics. Sudden drops of c_I measured for short lags, as in the top trace of Fig.0.2c, are indicative of a sudden rearrangement event that has led to a loss of correlation between the intensity patterns recorded at times t and $t+\tau$. As the rearrangement event ceases, the degree of correlation recovers its typical level. At longer time lags (middle trace in Fig.0.2c), c_I has a highly fluctuating behavior, because several events may occur during the probed lag. By contrast, almost no fluctuations are observed at very long lags (bottom trace in Fig.0.2c), since a large number of events has occurred for all pairs of images, leading to a full decorrelation.

Various way of characterizing the fluctuations of c_I have been proposed, including analyzing the probability distribution function and the moments of its fluctuations, or their temporal autocorrelation (Duri *et al.*, 2005). Here, we focus on the variance

$$\chi(\tau) = \mathrm{var}(c_I) \equiv \left\langle \left[c_I(t,\tau) - < c_I(t,\tau) >_t \right]^2 \right\rangle_t , \tag{0.7}$$

which is the analogous in light scattering of the dynamical susceptibility χ_4 discussed in detail in Chapter 2. Intuitively, one understands that large fluctuations of c_I must be associated to "rare", large events: if the rearrangements were very localized, many such events would be necessary to significantly decorrelate the light scattered by a macroscopic sample volume. Assuming independent events, the resulting spatial average would yield a smooth c_I trace. More precisely, χ can be shown to be proportional to the volume integral of the spatial correlation of the dynamics, as discussed for χ_4 in Chapter 2. An example of the scaling of χ with the size of the events for a coarsening foam, where events can be unambiguously identified, is discussed in (Mayer *et al.*, 2004) (see also Chapter 5). A few differences exist between χ in light scattering experiments and χ_4 in simulations or real space measurements. Contrary to χ_4, χ is not normalized with the respect to the number N of particles (compare Eq. (0.7) to eqn (11) in Chapter 3), since usually N is not known precisely in light scattering. Accordingly, typical

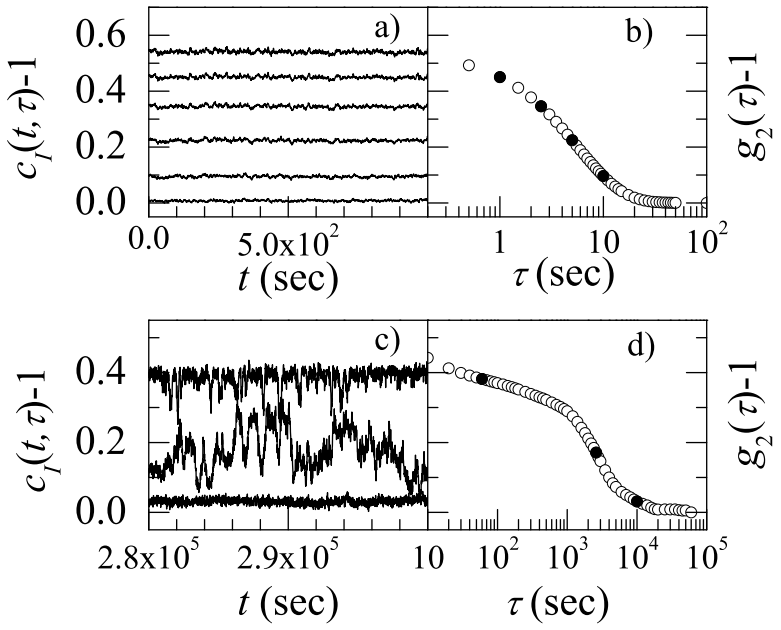

Fig. 0.2 a) Degree of correlation $c_I(t,\tau)$ for a diluted suspension of Brownian particles: the dynamics are stationary and homogeneous, as seen by the very small fluctuations of c_I, due uniquely to measurement noise. From top to bottom, $\tau = 0, 1, 2.5, 5, 10$ and 700 sec. b) Intensity correlation function $g_2 - 1$ obtained by averaging over time the data in a). The solid circles correspond to the time delays for which c_I is shown in a). c), d): degree of correlation and intensity correlation function for a colloidal gel (Duri and Cipelletti, 2006) (see Sec. 0.5.2). In c), $t = 0$ when the gel is formed. Note the large fluctuations of c_I, due to the heterogeneous nature of the dynamics. Individual events are discernable in the top trace ($\tau = 60$ sec), while the large fluctuations of the middle trace are due to the superposition of a fluctuating number of events ($\tau = 2600$ sec). For the bottom trace, $\tau = 10000$ sec

values reported for χ are much smaller than those for χ_4. Moreover, correction methods (Duri *et al.*, 2005) to remove the contribution of the statistical noise to χ are often used: using these corrections, one has $\chi = 0$ for homogeneous dynamics.

While time resolved correlation (TRC) experiments probe temporal fluctuations of the dynamics, they still lack spatial resolution. In photon correlation imaging (PCI), by contrast, spatial resolution is achieved by modifying the collection optics. As shown in (Duri *et al.*, 2009*b*) and sketched in Fig. 0.3 for $\theta = 90°$, a lens is used to image the scattering volume onto a CCD or CMOS detector, while a diaphragm limits the range of q vectors accepted by the detector. Under these conditions, each pixel of the sensor is illuminated by light issued from a small region of the sample and scattered in a small solid angle associated with the same, well defined scattering vector. The images are analyzed in the same way as for TRC, except that they are divided in regions of interest (ROIs): a local degree of correlation $c_I(\boldsymbol{r}, t, \tau)$ is calculated for each ROI, by averaging the intensity correlation function over a small set of pixels centered around

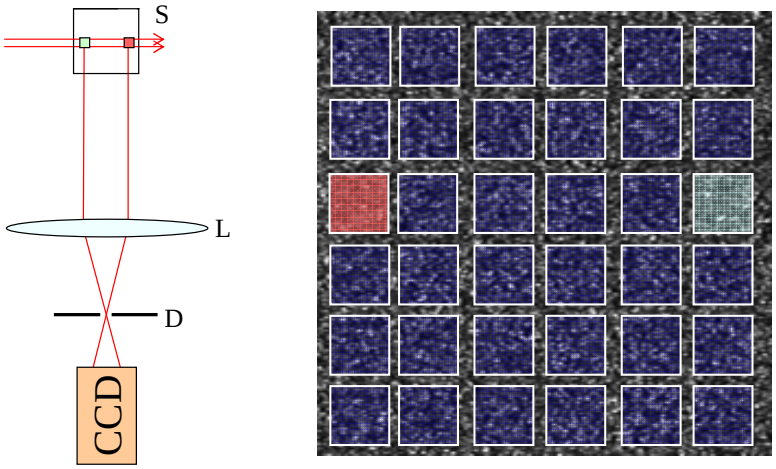

Fig. 0.3 left: scheme of the Photon Correlation Imaging apparatus for a scattering angle $\theta = 90°$. The lens L makes an image of the sample S onto the CCD detector. The diaphragm D, placed in the focal plane of L, selects only light rays scattered at $\theta \approx 90°$. Right: typical CCD image recorded by a PCI apparatus. The overlaid boxes indicate the grid of ROIs for which local degrees of correlation, $c_I(\boldsymbol{r}, t, \tau)$, are calculated. The size L of the ROIs has been exaggerated for the sake of clarity; typically, L is of the order of 10-20 pixels, corresponding to $\sim 20 - 100$ μm in the sample

$\boldsymbol{r}$. The spatial correlation of the dynamics can then be measured by comparing the temporal evolution of $c_I(\boldsymbol{r}, t, \tau)$ for ROIs separated by a distance $\Delta\boldsymbol{r}$. More specifically, we define (Duri *et al.*, 2009*b*)

$$g_4(\Delta\boldsymbol{r}, \tau) = B(\tau) \left\langle \frac{\langle \delta c_I(\boldsymbol{r}, t, \tau) \delta c_I(\boldsymbol{r} + \Delta\boldsymbol{r}, t, \tau) \rangle_t}{\sqrt{\mathrm{var}[\delta c_I(\boldsymbol{r}, t, \tau)] \mathrm{var}[\delta c_I(\boldsymbol{r} + \Delta\boldsymbol{r}, t, \tau)]}} \right\rangle_{\boldsymbol{r}} \tag{0.8}$$

where $\delta c_I = c_I - < c_I >_t$ are the temporal fluctuations of the local dynamics and $B(\tau)$ is a normalizing coefficient chosen so that $g_4(\Delta\boldsymbol{r}, \tau) \to 1$ as $\Delta\boldsymbol{r} \to 0$. This is the analogous, albeit at a coarse grained level, of the spatial correlation of the dynamics calculated in numerical and experimental work where particle trajectories are accessible (see Chapters 2 and 5). In most cases, the dynamics are isotropic and g_4 is averaged over all orientations of $\Delta\boldsymbol{r}$. It is important to distinguish the length scale over which the dynamics are probed from the spatial resolution with which the local dynamics can be measured. The former is dictated by the inverse scattering vector. Depending on the scattering angle, typical values range from a fraction of μm up to tens of μm. The latter is determined by the size of the ROIs and the magnification with which the sample is imaged. Typical values are in the range 20-100 μm. As a final remark, we note that the differential dynamic microscopy method (Cerbino and Trappe, 2008) mentioned at the end of Sec. 0.2.1 could be easily adapted to calculate g_4. This would improve the spatial resolution as compared to that of PCI, thanks to the larger magnification typically used in a microscope.

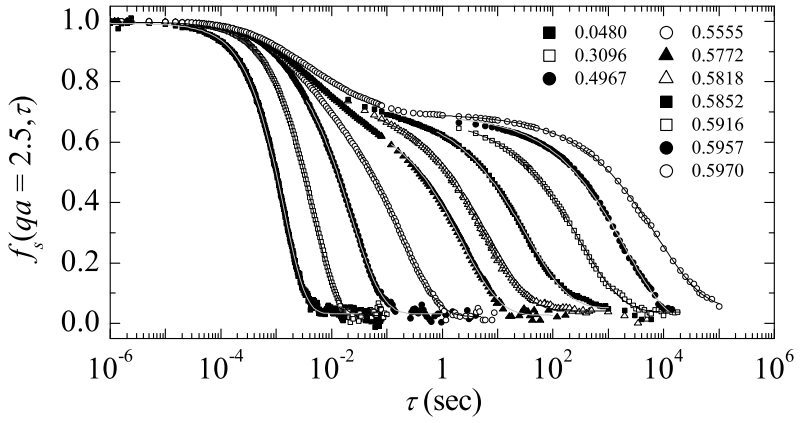

Fig. 0.4 Intermediate scattering functions for colloidal hard spheres (Brambilla *et al.*, 2009; Brambilla *et al.*, 2010). Data are labeled by the volume fraction φ. The lines are stretched exponential fits to the final decay of $f_s(q, \tau)$. Adapted from (Brambilla *et al.*, 2009) with permission

0.3 Average dynamics and dynamical heterogeneity in the supercooled regime

0.3.1 Structural relaxation time

The average dynamics of colloidal hard spheres in the supercooled regime ($\varphi < \varphi_g$) has been thoroughly studied in a series of works on PMMA-based systems (Pusey and van Megen, 1987; van Megen and Underwood, 1994; van Megen *et al.*, 1998; Brambilla *et al.*, 2009; El Masri *et al.*, 2009). Figure 0.4 shows typical ISFs measured for a variety of volume fractions at a scattering vector $q = 2.5/a$ ($a = 100$ nm) (Brambilla *et al.*, 2009; Brambilla *et al.*, 2010), below the first peak of the static structure factor [we quote here the more precise determination of a reported in (Brambilla *et al.*, 2010), slightly smaller than that in (Brambilla *et al.*, 2009)]. These experiments are performed close to the best index matching conditions for a PMMA sample with size polydispersity $\sigma = 12.2\%$ (Brambilla *et al.*, 2010). Under these conditions the sample is optically polydisperse, as discussed in Sec. 0.2.3; thus, the self part of the ISF, f_s, is probed (El Masri *et al.*, 2009). At low volume fractions, the decay of f_s is well fitted by a single exponential, as expected for diluted Brownian particles. As φ increases, the ISFs develop a two-step relaxation. The initial decay depends weakly on φ and corresponds to the motion of a particle in the cage formed by its neighbors. The final decay corresponds to the relaxation of the cage; its characteristic time, τ_α, increases by almost 7 decades in the range of φ investigated, where all samples equilibrate.

Figure 0.5 shows $\tau_\alpha(\varphi)$, as obtained by fitting the final relaxation of the ISF to a stretched exponential:

$$f_s = B \exp[-(\tau/\tau_\alpha)^\beta] \,, \tag{0.9}$$

with $\beta \approx 0.56$ in the glassy regime. In the range $0.517 < \varphi < 0.585$, corresponding to about three decades in relaxation time, the volume fraction dependence of τ_α agrees

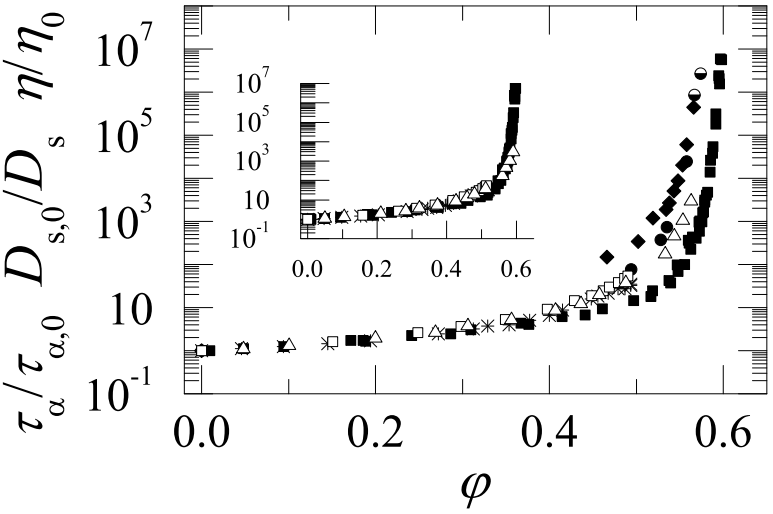

Fig. 0.5 Main panel: comparison of the volume fraction dependence of the structural relaxation time, self diffusion coefficient and low shear viscosity as determined in various works on PMMA colloidal hard spheres with size polidispersity ranging from $\approx$ 4% to 12.2%. All quantities are normalized with respect to their value in the $\varphi \to 0$ limit. Solid squares (Brambilla *et al.*, 2009), solid circles (van Megen and Underwood, 1994) and solid diamonds (van Megen *et al.*, 1998) are τ_α data obtained by DLS. Semifilled symbols indicate data where only a partial decay of $f(q,\tau)$ could be measured. Stars are self diffusion data obtained by DLS (Segrè *et al.*, 1995*c*). Open squares and open triangles are viscosity data from Refs. (Segrè *et al.*, 1995*c*) and (Cheng *et al.*, 2002), respectively. Inset: same data as a function of scaled volume fraction, where scaling factors ranging from 1 to 1.05 were chosen so as to superimpose all curves for $\varphi \leq 0.2$. [The data sets from Refs. (van Megen and Underwood, 1994; van Megen *et al.*, 1998), for which no low-φ data are available, are not included in this plot]. A reasonably good collapse is obtained also for $\varphi > 0.2$, suggesting that the main source of discrepancy between the various data sets lies in the uncertainty on the absolute volume fraction determination

very well with the critical law predicted by MCT (Gotze, 1999):

$$\tau_\alpha = \tau_0 \left(\frac{\varphi_c}{\varphi_c - \varphi} \right)^\gamma , \tag{0.10}$$

with $\gamma = 2.6$ and $\varphi_c = 0.59$. This is shown in Fig. 0.6a, where τ_α is plotted against $(1 - \varphi/\varphi_c)^{-1}$. Deviations are observed at low φ (as expected, since here MCT does not apply) and, more importantly, at the highest volume fractions that could be probed, where τ_α grows much slower than expected from MCT. This suggests that the divergence predicted by MCT is in fact avoided, as confirmed unambiguously by the fact that equilibrium ISFs could be measured up to $\varphi = 0.598$, above the critical packing fraction $\varphi_c = 0.59$ obtained from the MCT fit (Brambilla *et al.*, 2009;

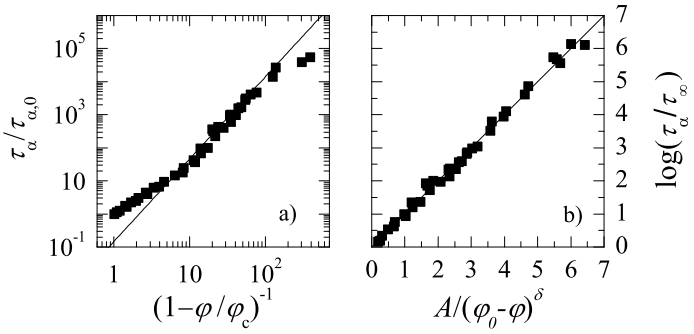

Fig. 0.6 a): double logarithmic plot of the structural relaxation time τ_α as a function of $(1-\varphi/\varphi_c)^{-1}$, where the critical volume fraction φ_c is obtained from a fit to Eq. (0.10) (adapted from (Brambilla *et al.*, 2009) with permission). In this representation, the MCT law is a straight line with slope $\gamma = 2.5$ (solid line). Data at $\varphi > \varphi_c$ are not represented in this plot. b): data from Ref. (Brambilla *et al.*, 2009) for $\varphi > 0.41$, plotted using reduced variable such that the generalized VFT law, Eq. (0.11) with $\varphi_0 = 0.637$ and $\delta = 2$, corresponds to the straight line shown in the plot (reproduced from (Brambilla *et al.*, 2009) with permission)

El Masri *et al.*, 2009). Figure 0.5 shows also data taken from previous works on PMMA systems (van Megen and Underwood, 1994; van Megen *et al.*, 1998), which exhibit a similar (apparent) algebraic divergence of τ_α. Note however that in these works data at very high φ could not be obtained, possibly explaining why the crossover between the MCT regime and the high φ "activated" regime reported in (Brambilla *et al.*, 2009; El Masri *et al.*, 2009) was not observed previously.

A similar crossover is observed in molecular glass formers (Donth, 2001): the reduced dynamical range accessible in colloids is responsible for the difficulty in pinpointing it, since typically φ_c is close to φ_g, the volume fraction above which equilibrium dynamics become too slow to be experimentally accessible. The analogy with molecular glass formers suggests that $\tau_\alpha(\varphi)$ may be fitted by a Vogel-Fulcher-Tammann (VFT)-like form:

$$\tau_\alpha = \tau_\infty \exp\left[\frac{A}{(\varphi_0 - \varphi)^\delta}\right], \tag{0.11}$$

where the exponent δ has been introduced for the sake of generality ($\delta = 1$ for the VFT law). Although a very good fit of the data of Ref. (Brambilla *et al.*, 2009) is obtained for $\delta = 1$, a somehow better fit is obtained for $\delta = 2$ and $\varphi_0 = 0.637$. The quality of the fit thus obtained can be appreciated in fig. 0.6b, where the data of Ref. (Brambilla *et al.*, 2009) are plotted using reduced variables so that Eq. (0.11) reduces to a straight line. A crucial question is whether φ_0 should be identified with $\varphi_{\rm RCP}$. Experimentally, this question is still open, due to the difficulties in measuring precisely the volume fraction at random close packing. Numerical simulations for a binary mixture of hard spheres (Berthier and Witten, 2009), however, show that $\varphi_0 = 0.641 < \varphi_{\rm RCP} \leq 0.664$ supporting the thermodynamic glass transition scenario and implying that in colloidal hard spheres the glass and the jamming transition are

distinct phenomena (Krzakala and Kurchan, 2007; Berthier and Witten, 2009). This viewpoint is still highly debated (see, e.g., (Xu *et al.*, 2009; Kamien and Liu, 2007)).

As a final remark on the structural relaxation in colloidal hard spheres, we note that one may wonder whether size polydispersity may have a significant impact on the dynamical behavior (van Megen and Williams, 2010; Brambilla *et al.*, 2010) and in particularly on the location of the (apparent) MCT divergence. Although no systematic experiments have been performed to address this issue (Williams and van Megen, 2001), computer simulations (El Masri *et al.*, 2009; Pusey *et al.*, 2009; Zaccarelli *et al.*, 2009*a*) have shown that φ_c is essentially unaffected by σ in the range $3\% < \sigma < 12\%$ typically explored in experiments.

0.3.2 Viscosity

Viscosity measurements are an alternative way to probe the average dynamics of hard sphere suspensions. Several works have been devoted to the φ dependence of the viscosity, η, in the limit of a vanishingly small applied shear, see e.g. Ref. (Cheng *et al.*, 2002) and references therein. These measurements are quite delicate, since the applied stress has to be very small (as low as a fraction of a mPa) in order to avoid non-linear effects, and because the resulting shear rate becomes extremely small beyond $\varphi \approx 0.5$, limiting measurements in the deeply supercooled regime. Additionally, the comparison between results obtained for different samples is affected by the uncertainties on the absolute volume fraction discussed above. Cheng *et al.* (Cheng *et al.*, 2002) show that data from various groups collapse reasonably well on a master curve when the absolute volume fractions are scaled by a factor up to about 1.03 to account for polydispersity. Figure 0.5 shows viscosity data from Refs. (Cheng *et al.*, 2002; Segrè *et al.*, 1995*c*) together with the DLS data discussed in Sec. 0.3.1. While there is some discrepancy between DLS and viscosity data, these differences are likely to be due, to a great extent, to uncertainties in φ and to the different methods used in the determination of the absolute volume fraction. Indeed, data sets for which data points at low φ are available can be scaled reasonably well onto a master curve by correcting φ using scaling factors between 1 and 1.05, so as to superimpose the growth of the viscosity or the relaxation time at low volume fraction ($\varphi \leq 0.2$) (see the inset of Fig. 0.5). The relationship between η and τ_α is discussed in more detail in Ref. (Segrè *et al.*, 1995*c*), where it is found that the low shear rate viscosity and the structural relaxation time measured by the collective ISF at the peak of the structure factor agree remarkably well up to $\varphi \sim 0.5$, while the relaxation time for the self part of the ISF is somehow lower.

The nature of the divergence of η is still a matter of debate. In their early work (Phan *et al.*, 1996), Russel, Chaikin and coworkers reported that $\eta(\varphi)$ is fitted well by the Krieger-Dougherty equation, a critical law of the same form as Eq. (0.10) with $\gamma = 2$, yielding $\varphi_c = 0.577$, consistent with the critical packing fraction obtained from MCT fits of DLS data. However, in their subsequent analysis of data on a larger range of viscosity (Cheng *et al.*, 2002), they report that a VFT-like fit (e.g. of the form of Eq. (0.11) with $\delta = 1$) yields better results. They find $\varphi_0 = 0.625$, close to random close packing, and significantly higher than φ_c. It should however be recalled that viscosity measurements are feasible only up to volume fractions lower than φ_c (e.g. $\varphi \leq 0.562$ in Ref. (Cheng *et al.*, 2002)),

making it difficult to draw unambiguous conclusions on the nature of the divergence of η, and in particular on the existence of a divergence at $\varphi_c \approx 0.58$.

0.3.3 Dynamical heterogeneity

The first microscopy experiment that examined the motion of supercooled colloidal particles was by Kasper, Bartsch, and Sillescu in 1998 (Kasper *et al.*, 1998). They devised a clever colloidal system primarily composed of refraction-index-matched particles made from cross-linked poly-*t*-butylacrylate. They then added a small concentration of tracer particles which had non-index-matched cores of polystyrene coated with shells of poly-*t*-butylacrylate. Using dark field microscopy, they could observe the motion of the tracer particles. They observed that particles exhibited caged motion, as described above in Sec. 0.3.1. That is, a particle would diffuse within some local region, trapped in a cage formed by its neighbors, and then occasionally exhibit a quicker motion to a new region. This was useful evidence that the dynamics are temporally heterogeneous, and the first direct experimental visualization of caged motion. Averaging over all of the tracer particles, they noted that the distribution of displacements was non-Gaussian, likely linked to the cage trapping and cage rearrangements. This experiment exploited an inherent size polydispersity of about 8% to prevent crystallization. The chief limitations of the experiment were that the observations were limited to two-dimensional slices of the three-dimensional sample, and also that only isolated tracer particles were observed, rather than every particle.

The next published experiment, by Marcus, Schofield, and Rice, had different tradeoffs (Marcus *et al.*, 1999). They used a very thin sample chamber to study a quasi-two-dimensional colloidal suspension; the spacing between the walls of their sample chamber was approximately 1.2 particle diameters. Because of the relative ease of studying a thin sample, they did not need tracer particles, but rather could follow the motion of every particle within the field of view. Like Ref. (Kasper *et al.*, 1998), they observed cage trapping and cage rearrangements, and found a non-Gaussian distribution of displacements. Being able to see all of the particles, they also noted that the cage rearrangement motions were spatially heterogeneous, with groups of particles exhibiting string-like motions. The string-like motions were quite similar to those seen in simulations (Kob *et al.*, 1997; Donati *et al.*, 1998; Hurley and Harrowell, 1996). Their results clearly showed a connection between the non-Gaussian behavior and the spatially heterogeneous dynamics, in that the non-Gaussian displacements were due to the particles involved in the cage rearrangements.

The experiment of Kegel and van Blaaderen in 2000 used confocal microscopy to improve upon the prior experimental limitations (Kegel and van Blaaderen, 2000). They observed the motion of core-shell colloidal particles, in a fully three-dimensional sample (although their observations were limited to two-dimensional images to maximize the imaging rate). Their colloidal samples were well-characterized as having hard-sphere interactions. In this experiment, they again observed string-like regions of high mobility, related to the non-Gaussian distribution of displacements. This was the first experiment to directly visualize spatially heterogeneous dynamics in a three-dimensional sample, confirming what simulations had already suggested, that string-like motion

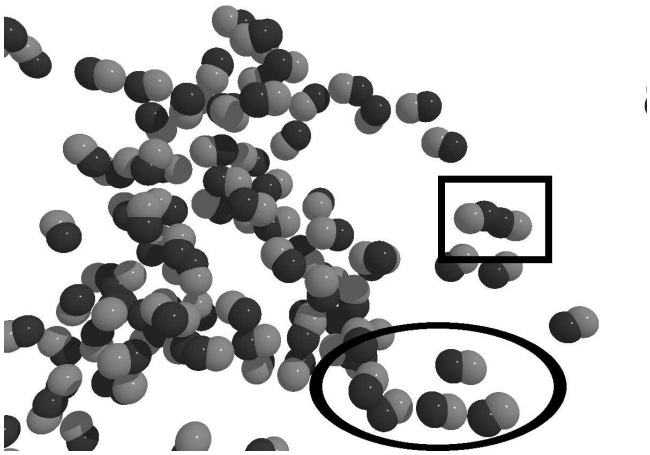

Fig. 0.7 Picture depicting the current positions of the most mobile colloidal particles (light colored) and the direction they are moving in (dark colored). The particles are drawn at 75% of their correct size, and for clarity only the most mobile particles are shown. Many particles move in similar directions to their neighbors, as shown by those within the oval. However, some particles also move in opposite directions to their neighbors, for example closing gaps between them, as highlighted by the rectangle. This is a sample with $\varphi = 0.56$, data taken from Ref. (Weeks *et al.*, 2000). The particles have radius $a = 1.18$ μm and the time scale used to determine the mobility is $\Delta t = 1000$ s

is not an artifact of two dimensional systems (Marcus *et al.*, 1999; Kob *et al.*, 1997; Donati *et al.*, 1998; Hurley and Harrowell, 1996; Perera and Harrowell, 1999).

Shortly after Ref. (Kegel and van Blaaderen, 2000), Weeks *et al.* published a similar experiment using confocal microscopy to study three-dimensional colloidal samples (Weeks *et al.*, 2000). Utilizing a faster confocal microscope than Ref. (Kegel and van Blaaderen, 2000), they were able to observe displacements in three dimensions. They too saw string-like motion, although also noted that some particles were moving in non-string-like ways termed "mixing" (Weeks and Weitz, 2002); see Fig. 0.7. A limitation of this experiment is that the particles were later discovered to be slightly charged, rather than being ideal hard spheres (Gasser *et al.*, 2001). The three-dimensional observations enabled the fractal nature of the regions of mobile particles to be measured as $d_f = 1.9 \pm 0.4$, similar to simulations (Donati *et al.*, 1999). The sizes of the mobile regions increased dramatically as the colloidal glass transition was approached.

Subsequently, the data of Ref. (Weeks *et al.*, 2000) has been reanalyzed to highlight other features. The idea of caging was quantified in Ref. (Weeks and Weitz, 2002), finding a result similar to Kasper *et al.* (Kasper *et al.*, 1998), that caging manifested itself as an anti-correlation of particle displacements in time. That is, if a particle pushed against the "walls" of its cage (formed by its neighbors), then the particle was likely to subsequently be pushed backwards. The original work of Ref. (Weeks *et al.*, 2000) highlighted mobile regions using a slightly arbitrary definition of which particles were

mobile. Later analysis used spatial correlation functions to avoid defining a particular subset of particles as mobile (Weeks *et al.*, 2007). These correlation functions found length scales for particle mobility which grew by a factor of 2 as the glass transition was approached, finding the largest length scale for a super-cooled liquid of approximately $8a$ in terms of the particle radius a.

More recent work has taken the study of dynamical heterogeneities in colloidal suspensions in new directions. One notable set of experiments uses superparamagnetic particles and an external magnetic field to control the glassiness of a sample *in situ* (König *et al.*, 2005; Ebert *et al.*, 2009; Mazoyer *et al.*, 2009). Other experiments study the colloidal glass transition in confinement (Nugent *et al.*, 2007), or glassy samples as they are sheared (Besseling *et al.*, 2007; Schall *et al.*, 2007; Chen *et al.*, 2010).

Dynamical heterogeneity in the equilibrium regime has also been probed by DLS. Attempts to directly measure χ_4 or g_4 using the time- and space-resolved methods discussed in Sec. 0.2.4 have, so far, failed, because these techniques lack the resolution needed to detect dynamical heterogeneity on the length scale of a few particles. By contrast, χ_4 can be measured indirectly using the theory developed in Chapter 3 (see Sec. 3.2.5 therein). For colloidal hard spheres the following relation holds (Berthier *et al.*, 2005; Berthier *et al.*, 2007*b*; Berthier *et al.*, 2007*a*):

$$\chi_4(q,\tau) = \chi_4(q,\tau)|_\varphi + \rho k_B T \kappa_T [\varphi \chi_\varphi(q,\tau)]^2, \tag{0.12}$$

where ρ is the number density, κ_T the isothermal compressibility (taken from the Carnahan-Starling equation of state), $\chi_4(q,\tau)|_\varphi$ denotes the value taken by $\chi_4(q,\tau)$ in a system where density is strictly fixed, and $\chi_\varphi(q,\tau) \equiv \partial f_s(q,\tau)/\partial\varphi$. Only the second term in the r.h.s. of Eq. (0.12) can be accessed experimentally. Numerical simulations, where both terms in the r.h.s. of (0.12) can be calculated (Brambilla *et al.*, 2009), show that the first term can be neglected in the deep supercooled regime: $\chi_4(q,\tau) \approx \rho k_B T \kappa_T [\varphi \chi_\varphi(q,\tau)]^2$ when the latter term is larger than unity. Experimentally, χ_φ can be obtained either by numerical differentiation using two ISFs measured at close enough volume fractions (see Fig. 0.8a), or by using the chain rule in the r.h.s. of Eq. (0.9):

$$\frac{\partial f_s}{\partial \varphi} = \frac{\partial f_s}{\partial B}\frac{\partial B}{\partial \varphi} + \frac{\partial f_s}{\partial \tau_\alpha}\frac{\partial \tau_\alpha}{\partial \varphi} + \frac{\partial f_s}{\partial \beta}\frac{\partial \beta}{\partial \varphi}, \tag{0.13}$$

where the partial derivatives with respect to volume fraction of the coefficients B, τ_α and β defined in Eq. (0.9) are obtained by fitting their φ dependence by smooth polynomials (Dalle Ferrier *et al.*, 2007; Brambilla *et al.*, 2009).

Figure 0.8a shows $\chi_4(q = 2.5a, \tau)$ together with the ISFs used to obtain it by finite difference (Berthier *et al.*, 2005), for the same system as in Ref. (Brambilla *et al.*, 2009). The dynamical susceptibility has the characteristic peaked shape observed in a variety of glassy systems (see also Chapters 2 and 5), with the maximum of the fluctuations, $\chi^* \equiv \chi_4(\tau^*)$, occurring on a time scale τ^* comparable to the structural relaxation time τ_α. As discussed in detail in Chapters 2 and 5, χ^* is of order $N_{\rm corr}$, the number of particles that undergo correlated rearrangements. Figure 0.8b shows χ^*, obtained for the same system but using the chain rule (0.13), as a function of φ. The amplitude of dynamical fluctuations increases with volume fraction, supporting theoretical scenarios where a growing dynamical length accompanies the divergence of the relaxation time

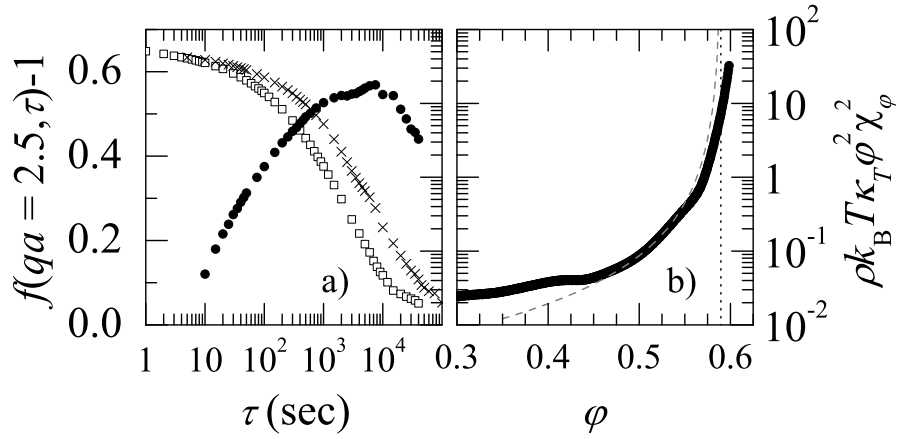

Fig. 0.8 a), left axis: ISFs at two nearby volume fractions ($\varphi = 0.5953$ and 0.5970 for the open squares and the crosses, respectively). The solid circles are χ_φ as obtained by finite difference from the two ISFs (right axis, same scale as in b)). b): height of the peak of χ_4, χ^*, as a function of φ (adapted from (Brambilla *et al.*, 2009) with permission). Here, χ_4 has been estimated using the chain rule, as explained in the text. The dashed line is a MCT fit to the dynamical susceptibility. The vertical dotted line indicates the location of the divergence predicted by MCT but avoided by the data

on approaching a glass transition. The dashed line shows the predictions of advanced mode coupling theories, $\chi^* \sim (\varphi_c - \varphi)^{-2}$ (Berthier *et al.*, 2007*b*; Berthier *et al.*, 2007*a*; Biroli and Bouchaud, 2004). As observed for the average dynamics, the data agree with MCT only over a limited range of volume fractions; in particular, MCT overpredicts the growth of χ^* at high φ, where the data remain finite across the the critical volume fraction φ_c. Therefore, the analysis of dynamical fluctuations confirms the crossover from an MCT regime to an activated regime at high volume fractions inferred from the average dynamics.

0.4 Average dynamics and dynamical heterogeneity in non-equilibrium regimes

0.4.1 The glassy regime

Thus far we have focused on dynamical heterogeneities in supercooled colloidal liquids; these systems will crystallize after some time (if the particles are sufficiently monodisperse). For polydisperse systems, the dynamics can be stationary (unless the sample has been recently sheared or stirred), since the sample is in (metastable) equilibrium. In contrast, glasses (volume fraction $\varphi > \varphi_g$) are out of equilibrium, and their properties depend on time, a phenomenon termed "aging." In particular, consider a low volume fraction colloidal suspension which is centrifuged to rapidly increase its volume fraction to the point where it becomes a colloidal glass at some time $t_w = 0$. The motion of particles within this sample depends on the time t_w since this formation, called

the waiting time or simply the age of the sample. Initially, particles can move relatively rapidly, but as the system ages, particle motion slows (van Megen *et al.*, 1998). Particles take longer to move the same distance that was covered quickly at an earlier age. Equivalently, the cages formed by a particle's neighbors are more long-lasting, and given that these samples have a high volume fraction, particles spend almost all of their time tightly confined within their cages.

In the earliest microscopy experiments (Ref. (Kasper *et al.*, 1998)), there was evidence of slow motion within glassy samples. While the mean square displacement of the particles grew extremely slowly, it did grow. This provided some evidence that particles were not completely frozen, but rather moved to new positions as the sample aged.

More direct observations were obtained via confocal microscopy in Ref. (Weeks *et al.*, 2000). In that experiment, Weeks *et al.* observed that while mobile regions of particles grew larger as $\varphi \to \varphi_g$ (in the super-cooled state), in glassy samples the mobile regions were quite small. This implied that spatial dynamical heterogeneities were less important for colloidal glasses. This result was revised in 2003 by Courtland and Weeks, who observed larger clusters of mobile particles in an aging colloidal glass, again using confocal microscopy (Courtland and Weeks, 2003). The key difference was in the data analysis. In a glassy sample, most of the particle motion is Brownian motion within the cages. Occasionally particles have cage rearrangements, but this is hard to distinguish from the Brownian motion as the distances particles move during these rearrangements gets very small (Weeks and Weitz, 2002; Courtland and Weeks, 2003). Courtland and Weeks were able to observe the cage rearrangements by low-pass filtering the raw trajectories, thus smoothing out the Brownian motion and making the cage rearrangements clearer. They found that there was indeed spatially heterogeneous dynamics comparable to the behavior of super-cooled colloids, but surprisingly they did not see any dependence on the aging time t_w. Similar results were also seen in a later confocal microscopy study of a binary colloidal glass (Lynch *et al.*, 2008).

One important consideration for studies of the aging of colloidal glasses is the protocol for achieving the initial glassy state. In traditional molecular glasses, a sample is quenched from a liquid state by rapidly reducing the temperature. In a colloidal glass, the analogous quench would be to rapidly increase the volume fraction, for example by centrifugation. However, in the experiments described above (Courtland and Weeks, 2003; Lynch *et al.*, 2008), the samples were instead prepared at a constant volume fraction, and then shear-melted by stirring them with an embedded stir bar. This is sometimes termed "shear-rejuvenation" as the stirring will make a well-aged colloidal glass look like a young colloidal glass, that is, it resets $t_w = 0$. However, there is evidence that these two protocols give different glassy states in molecular glassformers (McKenna, 2003).

Motivated by this, two groups have found ways to quench a colloidal glass *in situ* from a low volume fraction state to a high volume fraction state. One method uses an external magnetic field to control the effective inter-particle attraction in a two-dimensional colloidal sample composed of superparamagentic particles (Assoud *et al.*, 2009). This technique has not been used to study aging explicitly, but so far has focused on slow crystallization after a rapid quench (Assoud *et al.*, 2009). Another method uses

the sample temperature to control swelling in hydrogel particles, again in a quasi-two-dimensional experiment (Yunker *et al.*, 2009). Experiments using soft swellable particles are described in Sec. 0.5.1.

Dynamical heterogeneity in glassy colloidal samples have also been probed by DWS. We recall that this light scattering technique is sensitive to motion on very small length scales, down to a fraction of a nm (see Sec. 0.2.3), a highly desirable feature for glassy systems where particles hardly move. Reference (Ballesta *et al.*, 2008*b*) discusses both the average dynamics and its temporal fluctuations in very dense suspensions of relatively large particles ($a \approx 10$ μm). After initializing the sample by shaking it vigorously, the dynamics slow down until a pseudo-stationary regime is attained, where all measurements are performed. This regime does not correspond to a true equilibrium state, but rather to a regime where the very local dynamics probed in this experiment do not evolve significantly on the time scale of the experiments (up to a few days). Figure 0.9 shows the volume fraction dependence of various parameters characterizing the dynamics in the pseudo-stationary regime. As shown in a), the average relaxation time of the intensity correlation function, as obtained from a fit $g_2(t,\tau) - 1 = B \exp[-(\tau/\tau_0(t))^{\beta(t)}]$, increases smoothly with φ, seemingly diverging at $\varphi = \varphi_{\max} = 0.752$, presumably the random close packing volume fraction for this quite polydisperse system. Panel b) shows the φ dependence of the average stretching exponent, $\overline{\beta}$, which increases from about 0.9 to 1.3 as random close packing is approached. Panel c) shows the height, χ^*, of the peak of the dynamic susceptibility χ defined in Eq. (0.7). Quite surprisingly, χ^* is non-monotonic: it first increases with φ, reaches a maximum, but eventually drops dramatically close to random close packing.

The interpretation of these data requires special care, since the usual DWS formalism has been developed for spatially and temporally homogeneous dynamics. By contrast, Ref. (Ballesta *et al.*, 2008*b*) discusses a general model for DWS for heterogeneous dynamics, based on an extension of the formalism originally proposed by Durian *et al.* for DWS measurements of the spatially localized, temporally intermittent dynamics of a foam (Durian *et al.*, 1991). According to the model of (Ballesta *et al.*, 2008*b*), the non-monotonic behavior of $\chi^*(\varphi)$ results from the competition between two contrasting effects. On the one hand, the size ξ of the regions that undergo a rearrangement increases continuously with volume fraction, leading to enhanced temporal fluctuations as observed in supercooled samples (see Sec. 0.3.3). On the other hand, as φ increases the particle displacement associated with each of these events is increasingly restrained, due to crowding. Thus, an increasingly large number of rearrangement events is required to decorrelate the scattered light at high φ, leading to reduced fluctuations. While simple simulations of a DWS experiment in a medium undergoing rearrangements described by this scenario reproduce the experimental data (Ballesta *et al.*, 2008*b*), a direct measurement of $\xi(\varphi)$ would be necessary to confirm it. This would allow one to better understand analogies and differences with the experiments on driven grains (Lechenault *et al.*, 2008) mentioned in Chapter 5, where a non-monotonic behavior of *both* χ^* and ξ has been reported.

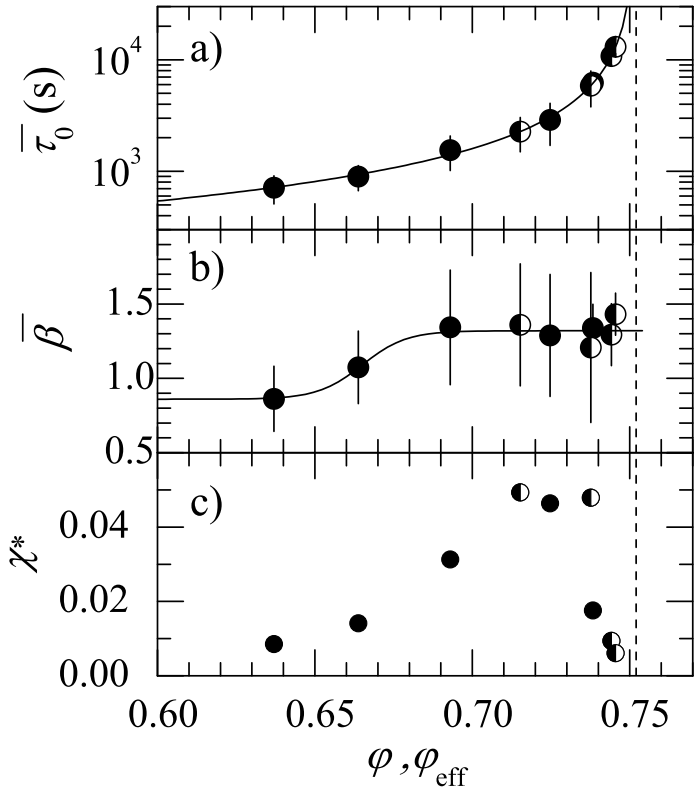

Fig. 0.9 Volume fraction dependence of the dynamics and its temporal fluctuations for a concentrated suspension of colloids as probed by DWS. Solid symbols refer to fresh samples, semi filled symbols to aged samples that have been rejuvenated mechanically. See (Ballesta *et al.*, 2008*b*) for more details. a) Average relaxation time, the line is a critical law fit to the data, $\overline{\tau_0} \sim (\varphi_{\rm max} - \varphi)^{-y}$ with $\varphi_{\rm max} = 0.752$ and $y = 1.5$. Here and in the other panels the vertical dashed line indicates the location of $\varphi_{\rm max}$. b) Stretching exponent obtained by fitting the final relaxation of the intensity correlation function to a stretched exponential. c) Height χ^* of the peak of the dynamical susceptibility, $\chi(\tau)$. Note the abrupt drop of χ^* on approaching $\varphi_{\rm max}$. In a) and b), the bars indicate the standard deviation of the temporal distribution of the relaxation time and the stretching exponent, respectively. Adapted from Ref. (Ballesta *et al.*, 2008*b*) with permission

0.4.2 Dynamical heterogeneity under shear

Aging systems are out of equilibrium; another type of non-equilibrium system is a driven system. Of particular interest are samples that are sheared. The importance of shear can be quantified by a Péclet number (see also Sec. 0.1.2). This is the ratio of the time scale for diffusion to the time scale for shear-induced motion. The shear induced time scale is given in terms of the strain rate as $1/\dot{\gamma}$. Recall that the Brownian time scale is $\tau_B = a^2/(6D)$ (Eq. (0.1)). Typically when considering dense colloidal

suspensions, the relevant diffusion constant is D_∞, the long-time diffusion constant, which varies with the volume fraction. The other option would be to use D_0, as given by the Stokes-Einstein-Sutherland formula, Eq. (0.2), which is the diffusion constant in the $\varphi \to 0$ limit. If D_0 is used, the Péclet number is termed the bare Péclet number, Pe, and if D_∞ is used, it is termed the modified Péclet number, Pe^*. Given that we wish to understand how particles move and rearrange, this is the long-time-scale motion (D_∞), and combining the expressions above we find $Pe^* = a^2\dot{\gamma}/(6D_\infty)$. For $Pe^* < 1$, diffusion is the primary influence on particle motion, and the shear is only a small perturbation. For $Pe^* > 1$, the shear-induced motion is expected to be more significant. The main consideration here is that for the shear rate to be significant, an experiment must have $Pe^* > 1$, which is the case for the experiments described below in this subsection.

Simulations of supercooled fluids found that as Pe^* increases, the system becomes more-liquid like, and dynamically heterogeneous regions become smaller (Yamamoto and Onuki, 1997), similar to the idea of shear unjamming a sample (Liu and Nagel, 1998). As yet, this relationship between Pe^* and dynamical heterogeneity has been untested by colloidal experiments.

A complementary question is to ask what the nature of a shear-induced motion is, for a dense amorphous sample. For example, sheared crystalline materials respond by the internal motion of dislocation lines. Influential simulations by Falk and Langer found, for amorphous materials, that rearrangements occurred in localized regions, termed "shear transformation zones" (Falk and Langer, 1998). In these regions, locally the stress builds up until it is released by a rapid local rearrangement event. These behaviors have been directly observed in an experiment by Schall *et al.*, where they used confocal microscopy to examine a colloidal glass as it was sheared between two parallel plates at low strains $\sim 4\%$ (Schall *et al.*, 2007). In their experiment, the shear-induced dynamical heterogeneities had a small spatial extent, although in some cases they appeared to relax the strain over a large region even though the farther away particles did not move very far. Their activation energy was estimated to be $E \sim 16k_BT$, where k_BT is the thermal energy. Given the low strain, it is possible that these observations are of shear-induced aging effects, rather than shear flow.

A separate experiment examined the shear-induced motion of colloidal particles in supercooled colloidal liquids (Chen *et al.*, 2010). In these less dense samples, localized rearranging regions were observed at high strain values. These samples were sheared between two parallel plates that moved back and forth with a triangle wave displacement curve. Strikingly, the shapes of these rearranging regions were isotropic on average, and showed no distinction between the velocity direction, velocity gradient direction, and the vorticity direction mutually perpendicular to the first two. Similar observations were made of a sheared colloidal glass (Besseling *et al.*, 2007): in those experiments, little difference was found in the effective diffusivity in the three directions, once the affine motion of the average shear profile was subtracted from the particle displacements. This study was the first direction observation of a sheared colloidal glass which directly imaged shear-induced dynamical heterogeneities (Besseling *et al.*, 2007). Note that the isotropic nature of plastic rearrangements observed in experiments is at odds with recent simulations of a 2D supercooled fluid of soft particles, where anisotropic

structural rearrangements were observed (Furukawa *et al.*, 2009). These observations depended on careful analysis methods, which have not yet been applied to experimental data from colloids.

While not directly the same idea as shear-induced dynamical heterogeneity, it is important to note that many soft glassy systems – such as colloids – exhibit shear-banding (Dhont, 1999; Dhont *et al.*, 2003; Fielding, 2007; Dhont and Briels, 2008; Fielding *et al.*, 2009). That is, when a large sample is sheared, sometimes the strain is localized near one of the boundaries. Within the "shear band" the sample is straining a significant amount and plastically deforming, while outside the shear band, the sample is nearly unstrained. As the stress must be continuous throughout the sample, this suggests that the material is acting as if it has two states, a low viscosity state in the shear band where the sample flows, and an elastic state outside the shear band without flow. Shear bands have been noted in colloidal suspensions (Vermant, 2001; Chen *et al.*, 2010; Besseling *et al.*, 2007; Ballesta *et al.*, 2008*a*; Dhont and Briels, 2008), colloidal gels (Moller *et al.*, 2008), worm-like micelles (Berret *et al.*, 1997; Olmsted, 1999; Cates and Fielding, 2006), foams (Debrégeas *et al.*, 2001; Lauridsen *et al.*, 2004; Janiaud *et al.*, 2006), and granular materials (Losert *et al.*, 2000; Utter and Behringer, 2008). Note that the experiments discussed in the previous paragraph (Ref. (Besseling *et al.*, 2007; Chen *et al.*, 2010)) were observations of a homogeneously shearing subregion within the shear band.

0.5 Beyond hard spheres

0.5.1 Soft particles

Colloidal particles with soft repulsive potential interactions can be obtained in several ways. One possibility is to exploit the softness of an electrostatic or magnetic repulsive potential. Another possibility is to modify the synthesis of the particles, e.g. in star polymers or microgel particles, where the degree of softness is governed by the number of arms and the degree of crosslinking, respectively. Finally, systems based on the self-assembly of amphiphilic molecules can form soft spheres, e.g. with amphiphilic diblock copolymers.

For soft systems, a nominal volume fraction, φ_{nom}, is often defined, based on the size of isolated particles and their number concentration; since particles can be squeezed, φ_{nom} can exceed unity. At low concentration, soft spheres behave similarly to hard spheres, provided that an effective size that takes into account the range of the soft repulsion is used. This is shown, e.g., by viscosity measurements (Roovers, 1994; Buitenhuis and Förster, 1997; Senff *et al.*, 1999), where the increase of the relative viscosity with concentration is essentially indistinguishable from that of hard spheres. At higher concentration, however, the behavior deviates significantly (Roovers, 1994; Buitenhuis and Förster, 1997; Sessoms *et al.*, 2009; Mattsson *et al.*, 2009*a*): the growth of the viscosity or the relaxation time with φ_{nom} is much gentler and samples with $\varphi_{\mathrm{nom}} > \varphi_{\mathrm{RCP}}$ may still be fluid, since particle deformations allow for structural relaxation.

In the past years, aqueous solutions of poly-N-isopropylacrylamide (PNiPAM) microgels are become one of the most popular soft systems. Not only can their softness be controlled during the synthesis (by varying the amount of crosslinking), but

it can also be tuned by varying the temperature, T. Under appropriate conditions, a decrease of a few degrees of T results in a $\sim$ 20% growth of the particle radius (Senff *et al.*, 1999) and in an increased softness. The influence of the softness of concentrated PNiPAM particles on their dynamics has been studied in detail by DLS in Ref. (Mattsson *et al.*, 2009*a*). Quite remarkably, the authors find that softness correlates with fragility, defined here as the slope of $\log \tau_\alpha$ *vs* concentration, ζ, at the glass transition, in analogy with the definition for molecular glass formers (Donth, 2001), where $1/T$ replaces ζ. Very soft particles have an Arrhenius-like behavior, $\tau_\alpha \sim \exp(C\zeta)$, harder particles have a larger fragility (steeper increase of $\tau_\alpha(\zeta)$), and hard spheres are the most fragile system, with the steepest increase of τ_α on approaching the glass transition. Thus, soft colloids appear as a promising system for understanding the origin of fragility in glasses, a long standing problem.

A similar system has been investigated by photon correlation imaging (PCI) in Ref. (Sessoms *et al.*, 2009). Both χ and g_4 have been studied as a function of $\varphi_{\rm nom}$ in measurements of the collective dynamics at low q. The amplitude of temporal fluctuations of the dynamics is found to increase monotonically with $\varphi_{\rm nom}$, while the range of spatial correlations of the dynamics has a non-monotonic behavior, a maximum being observed at $\varphi_{\rm nom} \approx \varphi_{\rm RCP}$. Remarkably, spatial correlations of the dynamics here extend over several mm, in analogy with what was reported for other jammed materials (see Sec. 0.5.2).

The T dependence of the size of PNiPAM particles provides a convenient way to quench them rapidly in a glassy state, by preparing a relatively concentrated —yet fluid— sample, which is then cooled by a few degrees, thereby swelling the particles to a quenched glassy state in a fraction of a second. This protocol was used in a quasi-two-dimensional experiment (Yunker *et al.*, 2009), where observations of aging over nearly six decades in aging time t_w were possible, due to the rapid quench rate. The authors observed spatial dynamical heterogeneity; particles occasionally underwent irreversible rearrangements. While the average size of the rearranging regions remained approximately constant during aging, similar to the prior study of 3D hard sphere samples (Ref. (Courtland and Weeks, 2003)), they identified an increase in the size of a particular class of rearranging regions as the sample aged. Specifically, the domain size of rearranging particles surrounding irreversible rearrangements increased during aging. The largest clusters of rearranging regions involved approximately 100 particles, a size much smaller than the range of dynamical correlations measured in (Sessoms *et al.*, 2009). However, the technique used to identify rearranging particles limited the correlation size, making direct quantitative comparisons difficult. Additionally, they saw a relation between the local structure and the particle motion, which agrees with some prior work on hard spheres (Cianci *et al.*, 2006).

0.5.2 Attractive particles

When colloidal particles experience attractive forces, arrested phases may be obtained also at a volume fraction lower than that required for glassy dynamics to be observed in hard spheres. The distinction is often made between colloidal gels (up to $\varphi \sim 0.3$) and attractive glasses (over $\varphi \sim 0.5$)(Trappe and Sandkuhler, 2004). Very recent work by Zaccarelli and Poon further refines the classification of concentrated attractive sys-

tems (Zaccarelli *et al.*, 2009*b*), based on the predominance of either caging or bonding. Concentrated, attractive glasses (Eckert and Bartsch, 2002; Pham *et al.*, 2002) have a structure similar to that of repulsive HS systems, while the structure of diluted gels depends on the strength of the interactions: highly attractive systems tend to form string-like, fractal structures, while gel strands are thicker when the interparticle potential well at contact is close to $k_{\mathrm{B}}T$ (Campbell *et al.*, 2005; Dibble *et al.*, 2006). The mechanism leading to gel formation is still intensely debated; recent work, still controverted, points to the role of an underlying fluid-fluid phase transition which is arrested once the dense phase becomes too concentrated (Lu *et al.*, 2008) (see Ref. (Zaccarelli, 2007) for a recent review on colloidal gels). Experimentally, attractive systems are typically realized either by screening the Coulomb repulsion in charge-stabilized systems, thereby exposing the particles to short range, attractive van der Waals forces (Russel *et al.*, 1992), or by means of the depletion force (Asakura and Oosawa, 1958; Vrij, 1976) induced by adding to the suspension smaller particles, often polymer coils (Poon, 2002).

Dynamical heterogeneity in weak gels have been explored mainly by confocal microscopy (Gao and Kilfoil, 2007; Dibble *et al.*, 2008) and simulations (Puertas *et al.*, 2004; Charbonneau and Reichman, 2007). The general picture emerging from these works is that DH is closely related to structural heterogeneity. The probability distribution function of the particles displacement (van Hove function) has typically a non-Gaussian shape, with "fat" tails corresponding to fast particles whose displacement is anomalously large (Gao and Kilfoil, 2007; Dibble *et al.*, 2008; Chaudhuri *et al.*, 2008). These particles are located at the boundaries of the thick strands constituting the gel, while the particles buried within the strands are the least mobile. A detailed analysis of particle mobility as a function of the number of their neighbors (Dibble *et al.*, 2008) confirms this picture. It should be noted that such a structural origin of DH is in contrast with hard sphere systems, where no clear connection between DH and structural quantities could be established so far. The influence of structure on dynamical heterogeneity in attractive systems has also been highlighted in a series of simulation papers by A. Coniglio and coworkers (see e.g. Ref. (Fierro *et al.*, 2008)).

The length scale dependence of dynamical heterogeneity in weak gels has been explored both numerically (Charbonneau and Reichman, 2007) and in XPCS experiments (Trappe *et al.*, 2007). In these works, the peak χ^* of the dynamical susceptibility χ_4 has been measured as a function of scattering vector q. χ^* has a non-monotonic behavior, the largest dynamical fluctuations being observed on a length scale of the order of the range of the attractive interparticle potential. This has to be contrasted to the case of repulsive systems, where the maximum of χ^* typically occurs around the interparticle distance (Charbonneau and Reichman, 2007; Dauchot *et al.*, 2005). On a more technical level, it is worth noting that Ref. (Trappe *et al.*, 2007) has demonstrated that modern synchrotron sources and X-ray detectors are now sufficiently advanced to allow for measurements of dynamical heterogeneities. The activity in this field is thus growing rapidly (Trappe *et al.*, 2007; Wandersman *et al.*, 2008; Herzig *et al.*, 2009; Duri *et al.*, 2009*a*; Wochner *et al.*, 2009) and there is hope that eventually X-ray scattering experiments may probe dynamical heterogeneity in molecular glass formers and not only for colloidal systems.

Optical microscopy studies of the dynamics of strong gels are difficult, due to the

restrained and very slow motion of particles in these systems (Dibble *et al.*, 2008). By contrast, scattering techniques have been successfully applied to characterize the slow dynamics of tenuous, fractal-like gels made of particles tightly bound by van der Waals forces (Cipelletti *et al.*, 2000; Duri and Cipelletti, 2006; Duri *et al.*, 2009*b*). Time resolved correlation (TRC, see Sec. 0.2.4) experiments show that the dynamics are due to intermittent rearrangement events where particles move over relatively small distances, of the order of a fraction of a μm (Duri and Cipelletti, 2006). Quite surprisingly, each of these events affects a macroscopic portion of the sample: the spatial correlation of the dynamics measured by photon correlation imaging (PCI, see Sec. 0.2.4) hardly decays over several millimeters, indicating that spatial correlations of the dynamics are limited essentially only by the system size (Duri *et al.*, 2009*b*). Once averaged over both time and space, the intensity correlation function $g_2(q,\tau)-1$ measured by "regular" multispeckle DLS exhibits a peculiar q dependence of both the relaxation time and the stretching exponent p obtained by fitting g_2-1 to a stretched exponential, $g_2(q,\tau)-1 \sim \exp[-(\tau/\tau_r)^p]$ (Cipelletti *et al.*, 2000). As shown in Fig. 0.10a, p is larger than one; accordingly, the relaxation has been termed a "compressed" exponential, as opposed to the as opposed to the stretched exponential relaxations often observed in glassy systems ($p<1$). Moreover, $\tau_r \sim q^{-1}$, as opposed to $\tau_r \sim q^{-2}$ as for diffusive motion.

In Refs. (Cipelletti *et al.*, 2000; Bouchaud and Pitard, 2002) these dynamics were interpreted as ultraslow ballistic motion due to the slow evolution of a strain field set by internal dipolar stresses. A more refined model has been proposed in Ref. (Duri and Cipelletti, 2006), taking into account the results from time- and space-resolved light scattering experiments that highlight the discontinuous nature of the relaxation process. The model is based on the following assumptions: i) the dynamics are due to individual rearrangement events that are random in time (Poissonian statistics); ii) each event affects the whole scattering volume (as indicated by PCI); iii) the displacement field induced by one single event is that due to the long-range elastic deformation of the gel under the action of dipolar stresses (in order to account for $p>1$); iv) on the length scales probed by the scattering experiments, the displacement due to successive events occurs along the same direction (i.e. the motion is, on average, ballistic-like, as implied by the scaling $\tau_r \sim q^{-1}$). The model contains just two adjustable parameters: the rate of the events in the scattering volume, γ, and the average particle displacement resulting from one single event, δ. The model captures well the q dependence of both p and τ_r as observed in the average dynamics, as shown in Fig. 0.10a. It also captures correctly the growing trend for the q dependency of the amplitude of dynamical heterogeneity, although it overestimates their magnitude by about a factor of two, as seen in Fig. 0.10b. Physically, the growth of dynamical heterogeneity with increasing q can be understood as the result of the competition between the length scale, q^{-1}, over which the dynamics is probed, and the typical particle displacement, δ, due to a rearrangement event. At very large q, $q\delta \geq 1$, one single event is sufficient to fully decorrelate g_2-1. In this regime, the instantaneous relaxation time depends on the time between successive events, which is a fluctuating quantity due to the Poissonian nature of the events. This yields very large fluctuations of the dynamics. As q decreases, an increasing number of events is required to decorrelate g_2-1, thus leading

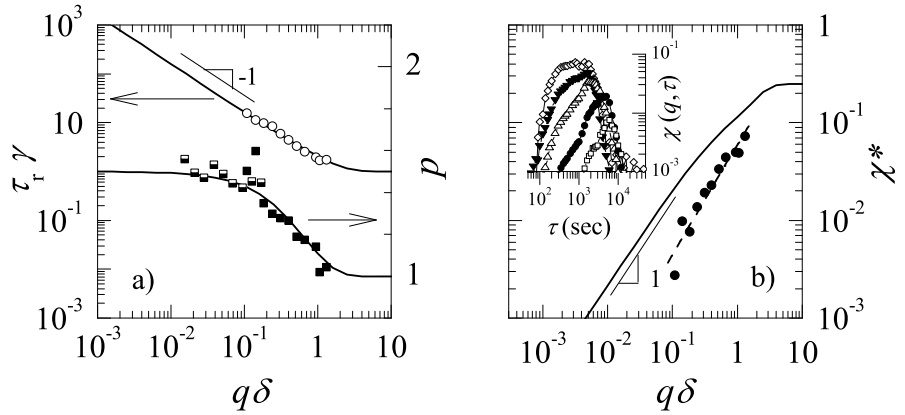

Fig. 0.10 Average dynamics and dynamical heterogeneity in a strong gel (adapted from (Duri and Cipelletti, 2006) with permission). a): q dependence of the relaxation time τ_r of the intensity correlation function (left axis, open circles) and of the stretching exponent (right axis, solid and semifilled squares). The data are normalized with respect to the parameters of the model (see also the text): $\delta = 250$ nm is the average particle displacement due to one single rearrangement event and $\gamma = (960\ \mathrm{s})^{-1}$ is the event rate. Note that the motion is, on average, ballistic-like ($\tau_r \sim q^{-1}$) and that the decay of $g_2 - 1$ is steeper than exponential ("compressed" exponential, $p \geq 1$). The lines are the predictions of the model. b) Inset: dynamical susceptibility $\chi(q, \tau)$ for various q. Main plot: q dependence of the height, χ^*, of the peak of $\chi(\tau)$. The dashed line is a power law fit with an exponent 1.13 ± 0.11, the solid line is the model

to smoother dynamics.

Quite intriguingly, the main features of the average dynamics reported for the strongly attractive gels discussed above have been also found in a large variety of glassy soft materials (for a review, see e.g. Ref.(Cipelletti and Ramos, 2005)). Models inspired by Ref. (Duri and Cipelletti, 2006) have been used also to describe the dynamics of nanoparticles embedded in molecular systems approaching the glass transition (Caronna *et al.*, 2008; Guo *et al.*, 2009). Moreover, photon correlation imaging experiments (Sessoms *et al.*, 2009; Maccarrone *et al.*,) on several systems (from concentrated soft spheres to repulsive glasses of charged clays and humidity-sensitive biofilms) suggest that system-spanning correlations of the dynamics may be a ubiquitous feature of jammed materials. This is in stark contrast with supercooled colloidal hard spheres, where spatial correlations of the dynamics extend over a few particle sizes at most, as discussed in Sec. 0.3.3. It is likely that the predominantly elastic behavior of jammed materials is responsible for the ultra-long spatial correlations of the dynamics observed in those systems, since the strain field set by a local rearrangement can propagate over large distances before being appreciably damped. Indeed, internal stress relaxation is often invoked as the origin of theses dynamics (Cipelletti *et al.*, 2000; Bouchaud and Pitard, 2002), although a complete understanding of the physical mechanisms underlying this peculiar yet general relaxation behavior is still lacking.

0.6 Perspectives and open problems

While the average dynamics of glassy colloidal systems has been intensively studied since the 1980's, experiments on dynamical heterogeneities started only about twelve years ago, spurred by advances in microscopy and light scattering methods and stimulated by numerical works. A (partial) list of what we have learned in the past years on both the average dynamics and dynamical heterogeneity of glassy colloids includes:

- Microscopy experiments have allowed us to observe directly what caged motion and cage rearrangements look like. Data have been used to quantify the meaning of "caging" (Weeks and Weitz, 2002).
- Scattering experiments have shed new light on the dynamics of concentrated hard spheres, for which equilibrium dynamics above the ergodic-non ergodic transition predicted by mode coupling theory have been reported (Brambilla *et al.*, 2009).
- A variety of microscopy and light scattering experiments agree on both the existence and the magnitude of dynamical heterogeneity in several colloidal systems, both 2D (Marcus *et al.*, 1999; König *et al.*, 2005; Ebert *et al.*, 2009; Mazoyer *et al.*, 2009) and 3D (Kasper *et al.*, 1998; Kegel and van Blaaderen, 2000; Weeks *et al.*, 2000), with both hard (Kegel and van Blaaderen, 2000; Weeks *et al.*, 2000) and soft (König *et al.*, 2005; Yunker *et al.*, 2009; Sessoms *et al.*, 2009) repulsive interactions. Along with simulations (Doliwa and Heuer, 1998; Donati *et al.*, 1998; Glotzer, 2000; Yamamoto and Onuki, 1998), this provides nice evidence that dynamical heterogeneities are ubiquitous in glassy systems and not artifacts of one particular colloidal system, one particular experimental technique, or one particular simulation method.
- Experiments on colloidal hard spheres have provided some of the first experimental quantitative evidence that the length scale of dynamical heterogeneities increases when approaching a glass transition (Weeks *et al.*, 2000; Berthier *et al.*, 2005; Weeks *et al.*, 2007).
- Light scattering experiments on deeply jammed attractive or soft repulsive systems (Ballesta *et al.*, 2008*a*; Sessoms *et al.*, 2009; Duri *et al.*, 2009*b*; Maccarrone *et al.*,) have unveiled a richer-than-expected scenario, with ultra-long ranged spatial correlations of the dynamics not observed so far in simulations.

In spite of these advances, several questions remain open, making dynamical heterogeneity an exciting field of research:

- Is there a structural origin of dynamical heterogeneity? While for diluted, attractive systems this has been shown to be the case, for concentrated, repulsive particles a clear answer is still lacking. Progress in this area will likely require the measurement of non-conventional structural quantities, e.g. the "point-to-set" correlation function introduced in numerical works (Biroli *et al.*, 2008) and discussed in Chapter 2.
- What is the behavior of dynamical heterogeneity in colloidal glasses and its relationship with aging? While recent work on soft particles suggests that the slowing down of the dynamics during aging may be associated with a growth of spatial correlations of the dynamics (Yunker *et al.*, 2009), this was not seen in experiments with harder spheres (Courtland and Weeks, 2003); this question requires further exploration.

- Is the non-monotonic φ dependence of dynamical fluctuations observed in some systems (Ballesta *et al.*, 2008*b*; Sessoms *et al.*, 2009) a general feature? Although a somehow similar behavior has been reported for granular systems (Lechenault *et al.*, 2008), the explanation proposed for colloids and grains are different: can these contrasting views be reconciled?
- Recent work (Duri *et al.*, 2009*b*; Sessoms *et al.*, 2009; Maccarrone *et al.*,) on jammed soft materials suggests that the relatively short-ranged correlation of the dynamics of supercooled hard spheres may be the exception rather than the rule, since system-size dynamical correlations are observed in those materials. What is the physical origin of these correlations? Why do the numerical simulations not capture these correlations?
- Most work on colloidal systems has been devoted to hard sphere-like systems. A general understanding of the role of the interaction potential on the slow dynamics and dynamical heterogeneity is still lacking. Recent experiments show that softer colloids have strikingly different behaviors than hard colloids (Mattsson *et al.*, 2009*b*), although these results are not fully understood.

Finally, we remark that numerical simulations can nowadays probe a range of relaxation times comparable to that explored by experiments (see e.g. (Brambilla *et al.*, 2009)). On the one hand, this calls for a more rigorous approach to the design of new experiments, since the question of what can be learned from experiments that simulations can not address needs to be asked. On the other hand, this opens the exciting possibility to compare in great detail numerical and experimental results, thereby allowing one to identify the physical mechanisms that are relevant in determining the slow relaxation of glassy colloidal systems.

0.7 Acknowledgements

The work of ERW was supported by NSF Grant No. CHE-0910707. The work of LC was supported by grants from ACI, ANR, CNRS, CNES, Région Languedoc-Roussillon, Institut Universitaire de France. LC acknowledges many discussions and fruitful collaborations with L. Berthier, G. Biroli, V. Trappe, and D.A. Weitz. ERW acknowledges helpful discussions and fruitful collaborations with J. C. Crocker and D. A. Weitz.

References

Adam, Gerold and Gibbs, Julian H. (1965). *J. Chem. Phys.*, **43**(1), 139–146.

Alcoutlabi, Mataz and McKenna, Gregory B. (2005, April). *J. Phys.: Cond. Matt.*, **17**(15), R461–R524.

Amblard, François, Yurke, Bernard, Pargellis, Andrew, and Leibler, Stanislas (1996). *Rev. Sci. Inst.*, **67**(3), 818–827.

Angell, C. A., Ngai, K. L., McKenna, G. B., McMillan, P. F., and Martin, S. W. (2000). *J. App. Phys.*, **88**(6), 3113–3157.

Antl, L., Goodwin, J. W., Hill, R. D., Ottewill, R. H., Owens, S. M., Papworth, S., and Waters, J. A. (1986, January). *Colloids and Surfaces*, **17**(1), 67–78.

Asakura, S. and Oosawa, F. (1958). *J. Polym. Sci.*, **33**(126), 183–192.

Assoud, Lahcen, Ebert, Florian, Keim, Peter, Messina, René, Maret, Georg, and Löwen, Hartmut (2009). *Phys. Rev. Lett.*, **102**(23), 238301.

Auer, Stefan and Frenkel, Daan (2001, October). *Nature*, **413**(6857), 711–713.

Axelrod, D., Koppel, D., Schlessinger, J., Elson, E., and Webb, W. (1976, September). *Biophys. J.*, **16**(9), 1055–1069.

Ballesta, P., Besseling, R., Isa, L., Petekidis, G., and Poon, W. C. K. (2008*a*). *Phys. Rev. Lett.*, **101**(25), 258301.

Ballesta, Pierre, Duri, Agnes, and Cipelletti, Luca (2008*b*, June). *Nature Physics*, **4**(7), 550–554.

Bandyopadhyay, R., Liang, D., Yardimci, H., Sessoms, D. A., Borthwick, M. A., Mochrie, S. G. J., Harden, J. L., and Leheny, R. L. (2004, Nov). *Phys. Rev. Lett.*, **93**(22), 228302.

Bartsch, E. (1995, December). *J. Non-Cryst. Solids*, **192-193**, 384–392.

Bartsch, E., Frenz, V., Baschnagel, J., Schärtl, W., and Sillescu, H. (1997). *J. Chem. Phys.*, **106**(9), 3743–3756.

Bartsch, E., Frenz, V., Moller, S., and Sillescu, H. (1993, December). *Physica A*, **201**(1-3), 363–371.

Beenakker, C. and Mazur, P. (1983, July). *Physica A: Statistical and Theoretical Physics*, **120**(3), 388–410.

Bernal, J. D. (1964, July). *Proc. Roy. Soc. London. Series A*, **280**(1382), 299–322.

Berne, B. J. and Pecora, R. (1976). *Dynamic Light Scattering*. Wiley, New York.

Berret, Jean F., Porte, Grégoire, and Decruppe, Jean P. (1997, Feb). *Phys. Rev. E*, **55**(2), 1668–1676.

Berthier, L., Biroli, G., Bouchaud, J. P., Cipelletti, L., Masri, D. El, L'Hote, D., Ladieu, F., and Pierno, M. (2005, December). *Science*, **310**(5755), 1797–1800.

Berthier, L., Biroli, G., Bouchaud, J. P., Kob, W., Miyazaki, K., and Reichman, D. R. (2007*a*). *J. Chem. Phys.*, **126**(18), 184504.

Berthier, L., Biroli, G., Bouchaud, J. P., Kob, W., Miyazaki, K., and Reichman, D. R.

(2007*b*). *J. Chem. Phys.*, **126**(18), 184503.
Berthier, L. and Tarjus, G. (2009, Oct). *Phys. Rev. Lett.*, **103**(17), 170601+.
Berthier, Ludovic and Witten, Thomas A. (2009, Aug). *Phys. Rev. E*, **80**(2), 021502.
Besseling, R., Isa, L., Weeks, E. R., and Poon, W. C. K. (2009, February). *Advances in Colloid and Interface Science*, **146**(1-2), 1–17.
Besseling, R., Weeks, Eric R., Schofield, A. B., and Poon, W. C. K. (2007). *Phys. Rev. Lett.*, **99**(2), 028301.
Biroli, G. and Bouchaud, J. P. (2004). *Europhys. Lett.*, **67**(1), 21–27.
Biroli, G., Bouchaud, J. P., Cavagna, A., Grigera, T. S., and Verrocchio, P. (2008, August). *Nature Physics*, **4**(10), 771–775.
Bolhuis, Peter G. and Kofke, David A. (1996, Jul). *Phys. Rev. E*, **54**(1), 634–643.
Bouchaud, J. P. and Pitard, E. (2002, November). *The European Physical Journal E - Soft Matter*, **9**(3), 287–291.
Brambilla, G., El Masri, D E. M., Pierno, M., Berthier, L., Cipelletti, L., Petekidis, G., and Schofield, A. B. (2009, Feb). *Phys. Rev. Lett.*, **102**(8), 085703.
Brambilla, G., Masri, D. El, Pierno, M., Berthier, L., Cipelletti, L., Petekidis, G., and Schofield, A. (2010, Apr). *Phys. Rev. Lett.*, **104**(16), 169602.
Buitenhuis, Johan and Förster, Stephan (1997). *J. Chem. Phys.*, **107**(1), 262–272.
Campbell, Andrew I., Anderson, Valerie J., van Duijneveldt, Jeroen S., and Bartlett, Paul (2005, May). *Phys. Rev. Lett.*, **94**(20), 208301.
Cardenas, Miguel, Franz, Silvio, and Parisi, Giorgio (1999). *J. Chem. Phys.*, **110**(3), 1726–1734.
Caronna, Chiara, Chushkin, Yuriy, Madsen, Anders, and Cupane, Antonio (2008, Feb). *Phys. Rev. Lett.*, **100**(5), 055702.
Castillo, H. E. and Parsaeian, A. (2007). *Nature Physics*, **3**(1), 26–28.
Cates, M. E. and Fielding, S. M. (2006). *Advances in Physics*, **55**(7/8).
Cerbino, Roberto and Trappe, Veronique (2008, May). *Phys. Rev. Lett.*, **100**(18), 188102.
Charbonneau, P. and Reichman, D. R. (2007, Sep). *Phys. Rev. Lett.*, **99**(13), 135701.
Chaudhuri, Pinaki, Berthier, Ludovic, and Sastry, Srikanth (2010, Apr). *Phys. Rev. Lett.*, **104**(16), 165701.
Chaudhuri, Pinaki, Gao, Yongxiang, Berthier, Ludovic, Kilfoil, Maria, and Kob, Walter (2008). *J. Phys.: Cond. Matt.*, **20**(24), 244126.
Chen, Dandan, Semwogerere, Denis, Sato, Jun, Breedveld, Victor, and Weeks, Eric R. (2010, Jan). *Phys. Rev. E*, **81**(1), 011403.
Cheng, Zhengdong, Zhu, Jixiang, Chaikin, Paul M., Phan, See-Eng, and Russel, William B. (2002, April). *Phys. Rev. E*, **65**(4), 041405.
Chung, B., Ramakrishnan, S., Bandyopadhyay, R., Liang, D., Zukoski, C. F., Harden, J. L., and Leheny, R. L. (2006, Jun). *Phys. Rev. Lett.*, **96**(22), 228301.
Cianci, Gianguido C., Courtland, Rachel E., and Weeks, Eric R. (2006, September). *Solid State Comm.*, **139**(11-12), 599–604.
Cianci, Gianguido C. and Weeks, Eric R. (2007). In *Reports of the Institute of Fluid Science*, Volume 19, pp. 51–56. Tohoku University.
Cipelletti, Luca, Bissig, H., Trappe, V., Ballesta, P., and Mazoyer, S. (2003, December). *J. Phys.: Condens. Matter*, **15**, S257–S262.

Cipelletti, Luca, Manley, S., Ball, R. C., and Weitz, D. A. (2000, Mar). *Phys. Rev. Lett.*, **84**(10), 2275–2278.

Cipelletti, Luca and Ramos, Laurence (2005, February). *J. Phys.: Cond. Matt.*, **17**(6), R253–R285.

Clusel, Maxime, Corwin, Eric I., Siemens, Alexander O. N., and Brujic, Jasna (2009, July). *Nature*, **460**(7255), 611–615.

Courtland, Rachel E. and Weeks, Eric R. (2003, January). *J. Phys.: Cond. Matt.*, **15**(1), S359–S365.

Crocker, John C. and Grier, David G. (1996, April). *J. Colloid Interf. Sci.*, **179**(1), 298–310.

Dalle Ferrier, C., Thibierge, C., Simionesco, C. Alba, Berthier, L., Biroli, G., Bouchaud, J. P., Ladieu, F., L'Hôte, D., and Tarjus, G. (2007, Oct). *Phys. Rev. E*, **76**(4), 041510.

Dauchot, O., Marty, G., and Biroli, G. (2005, Dec). *Phys. Rev. Lett.*, **95**(26), 265701.

de Schepper, I. M., Cohen, E. G. D., and Verberg, R. (1996, July). *Phys. Rev. Lett.*, **77**(3), 584.

Debrégeas, G., Tabuteau, H., and di Meglio, J. M. (2001, October). *Phys. Rev. Lett.*, **87**(17), 178305.

Dhont, Jan and Briels, Wim (2008, April). *Rheologica Acta*, **47**(3), 257–281.

Dhont, Jan K. G. (1999, Oct). *Phys. Rev. E*, **60**(4), 4534–4544.

Dhont, Jan K. G., Lettinga, M. Pavlik, Dogic, Zvonimir, Lenstra, Tjerk A. J., Wang, Hao, Rathgeber, Silke, Carletto, Philippe, Willner, Lutz, Frielinghaus, Henrich, and Lindner, Peter (2003). *Faraday Disc.*, **123**, 157–172.

Dibble, Clare J., Kogan, Michael, and Solomon, Michael J. (2006, Oct). *Phys. Rev. E*, **74**(4), 041403.

Dibble, Clare J., Kogan, Michael, and Solomon, Michael J. (2008, May). *Phys. Rev. E*, **77**(5), 050401.

Dinsmore, A. D., Weeks, E. R., Prasad, V., Levitt, A. C., and Weitz, D. A. (2001). *App. Optics*, **40**(24), 4152–4159.

Doliwa, B. and Heuer, A. (1998, June). *Phys. Rev. Lett.*, **80**(22), 4915–4918.

Doliwa, B. and Heuer, A. (2000, Jun). *Phys. Rev. E*, **61**(6), 6898–6908.

Donati, Claudio, Douglas, Jack F., Kob, Walter, Plimpton, Steven J., Poole, Peter H., and Glotzer, Sharon C. (1998, Mar). *Phys. Rev. Lett.*, **80**(11), 2338–2341.

Donati, Claudio, Glotzer, Sharon C., and Poole, Peter H. (1999, Jun). *Phys. Rev. Lett.*, **82**(25), 5064–5067.

Donev, Aleksandar, Stillinger, Frank H., and Torquato, Salvatore (2007). *J. Chem. Phys.*, **127**(12), 124509.

Donev, Aleksandar, Torquato, Salvatore, Stillinger, Frank H., and Connelly, Robert (2004, Oct). *Phys. Rev. E*, **70**(4), 043301.

Donth, E. (2001). *The Glass Transition*. Springer.

Duri, A., Autenrieth, T., Stadler, L. M., Leupold, O., Chushkin, Y., Grübel, G., and Gutt, C. (2009*a*, Apr). *Phys. Rev. Lett.*, **102**(14), 145701.

Duri, Agnès, Bissig, Hugo, Trappe, Véronique, and Cipelletti, Luca (2005, Nov). *Phys. Rev. E*, **72**(5), 051401.

Duri, A. and Cipelletti, L. (2006). *Europhys. Lett.*, **76**(5), 972–978.

Duri, A., Sessoms, D. A., Trappe, V., and Cipelletti, L. (2009*b*, Feb). *Phys. Rev. Lett.*, **102**(8), 085702.

Durian, D. J., Weitz, D. A., and Pine, D. J. (1991, May). *Science*, **252**(5006), 686–688.

Ebert, F., Dillmann, P., Maret, G., and Keim, P. (2009). *Rev. Sci. Inst.*, **80**(8), 083902+.

Eckert, T. and Bartsch, E. (2002, Aug). *Phys. Rev. Lett.*, **89**(12), 125701.

Ediger, M. D. (2000). *Annu. Rev. Phys. Chem.*, **51**(1), 99–128.

Ediger, M. D., Angell, C. A., and Nagel, S. R. (1996, January). *J. Phys. Chem.*, **100**(31), 13200–13212.

Einstein, A. (1905). *Annalen der Physik (Leipzig)*, **17**, 549–560.

El Masri, D., Brambilla, G., Pierno, M., Petekidis, G., Schofield, A. B., Berthier, L., and Cipelletti, L. (2009, July). *Journal of Statistical Mechanics: Theory and Experiment*, **2009**(07), P07015.

Ernst, Richard M., Nagel, Sidney R., and Grest, Gary S. (1991, April). *Phys. Rev. B*, **43**(10), 8070–8080.

Falk, M. L. and Langer, J. S. (1998, Jun). *Phys. Rev. E*, **57**(6), 7192–7205.

Fasolo, Moreno and Sollich, Peter (2004, Oct). *Phys. Rev. E*, **70**(4), 041410.

Fielding, Suzanne M. (2007). *Soft Matter*, **3**(10), 1262–1279.

Fielding, S. M., Cates, M. E., and Sollich, P. (2009). *Soft Matter*, **5**(12), 2378–2382.

Fierro, A., Gado, E. Del, Candia, A. De, and Coniglio, A. (2008, April). *Journal of Statistical Mechanics: Theory and Experiment*, **2008**(04), L04002.

Furukawa, Akira, Kim, Kang, Saito, Shinji, and Tanaka, Hajime (2009, Jan). *Phys. Rev. Lett.*, **102**(1), 016001+.

Gao, Y. and Kilfoil, M. L. (2007, Aug). *Phys. Rev. Lett.*, **99**(7), 078301.

Gasser, U., Weeks, Eric R., Schofield, Andrew, Pusey, P. N., and Weitz, D. A. (2001, April). *Science*, **292**(5515), 258–262.

Gleim, Tobias, Kob, Walter, and Binder, Kurt (1998, November). *Phys. Rev. Lett.*, **81**(20), 4404–4407.

Glotzer, Sharon C. (2000, September). *J. Non-Cryst. Solids*, **274**(1-3), 342–355.

Goodman, J. W. (2007). *Speckle phenomena in optics: theory and applications*. Roberts and Company, Englewood.

Gotze, Wolfgang (1999, March). *J. Phys.: Cond. Matt.*, **11**(10A), A1–A45.

Götze, W. and Sjögren, L. (1991, May). *Phys. Rev. A*, **43**(10), 5442–5448.

Götze, W. and Sjogren, L. (1992). *Rep. Prog. Phys.*, **55**(3), 241–376.

Grier, David G. (2003, August). *Nature*, **424**(6950), 810–816.

Guo, Hongyu, Bourret, Gilles, Corbierre, Muriel K., Rucareanu, Simona, Lennox, R. Bruce, Laaziri, Khalid, Piche, Luc, Sutton, Mark, Harden, James L., and Leheny, Robert L. (2009, Feb). *Phys. Rev. Lett.*, **102**(7), 075702.

Habdas, P., Schaar, D., Levitt, A. C., and Weeks, E. R. (2004). *Europhys. Lett.*, **67**(3), 477–483.

Hecksher, Tina, Nielsen, Albena I., Olsen, Niels B., and Dyre, Jeppe C. (2008). *Nature Physics*, **4**(9), 737–741.

Henderson, S. I. and van Megen, W. (1998, January). *Phys. Rev. Lett.*, **80**(4), 877–880.

Hernández-Guzmán, Jessica and Weeks, Eric R. (2009, September). *Proc. Nat. Acad. Sci.*, **106**(36), 15198–15202.
Herzig, E. M., Robert, A., van 't Zand, Cipelletti, L., Pusey, P. N., and Clegg, P. S. (2009, Jan). *Phys. Rev. E*, **79**(1), 011405.
Hodge, Ian M. (1995, March). *Science*, **267**(5206), 1945–1947.
Höfling, Felix, Munk, Tobias, Frey, Erwin, and Franosch, Thomas (2008). *J. Chem. Phys.*, **128**(16), 164517.
Hoover, William G. and Ree, Francis H. (1968). *J. Chem. Phys.*, **49**(8), 3609–3617.
Hurley, M. M. and Harrowell, Peter (1996). *J. Chem. Phys.*, **105**(23), 10521–10526.
Inoué, Shinya and Spring, Kenneth R. (1997, August). *Video Microscopy : The Fundamentals (The Language of Science)* (2nd edn). Springer.
Janiaud, E., Weaire, D., and Hutzler, S. (2006, Jul). *Phys. Rev. Lett.*, **97**(3), 038302.
Kamien, Randall D. and Liu, Andrea J. (2007, Oct). *Phys. Rev. Lett.*, **99**(15), 155501.
Kasper, A., Bartsch, E., and Sillescu, H. (1998, September). *Langmuir*, **14**(18), 5004–5010.
Kaufman, Laura J. and Weitz, David A. (2006). *J. Chem. Phys.*, **125**(7), 074716.
Kegel, W. K. (2000). *Langmuir*, **16**(3), 939–941.
Kegel, Willem K. and van Blaaderen, Alfons (2000, January). *Science*, **287**(5451), 290–293.
Kob, Walter, Donati, Claudio, Plimpton, Steven J., Poole, Peter H., and Glotzer, Sharon C. (1997, Oct). *Phys. Rev. Lett.*, **79**(15), 2827–2830.
König, H., Hund, R., Zahn, K., and Maret, G. (2005, November). *Euro. Phys. J. E*, **18**(3), 287–293.
Krzakala, Florent and Kurchan, Jorge (2007, Aug). *Phys. Rev. E*, **76**(2), 021122.
Lauridsen, John, Chanan, Gregory, and Dennin, Michael (2004, Jul). *Phys. Rev. Lett.*, **93**(1), 018303.
Lechenault, F., Dauchot, O., Biroli, G., and Bouchaud, J. P. (2008). *Europhys. Lett.*, **83**(4), 46003.
Liu, Andrea J. and Nagel, Sidney R. (1998, November). *Nature*, **396**(6706), 21–22.
Liu, Cliff Z. and Oppenheim, Irwin (1996, January). *Phys. Rev. E*, **53**(1), 799–802.
Losert, W., Bocquet, L., Lubensky, T. C., and Gollub, J. P. (2000). *Phys. Rev. Lett.*, **85**(7), 1428–1431.
Lu, Peter J., Zaccarelli, Emanuela, Ciulla, Fabio, Schofield, Andrew B., Sciortino, Francesco, and Weitz, David A. (2008, May). *Nature*, **453**(7194), 499–503.
Lynch, Jennifer M., Cianci, Gianguido C., and Weeks, Eric R. (2008). *Phys. Rev. E*, **78**(3), 031410.
Maccarrone, S., Brambilla, G., Pravaz, O., Duri, A., Ciccotti, M., Fromental, J. M., Pashkovski, E., Lips, A., Sessoms, D., Trappe, V., and Cipelletti, L.
Marcus, Andrew H., Schofield, Jeremy, and Rice, Stuart A. (1999, Nov). *Phys. Rev. E*, **60**(5), 5725–5736.
Mason, T. G. and Weitz, D. A. (1995, Oct). *Phys. Rev. Lett.*, **75**(14), 2770–2773.
Mattsson, Johan, Wyss, Hans M., Fernandez-Nieves, Alberto, Miyazaki, Kunimasa, Hu, Zhibing, Reichman, David R., and Weitz, David A. (2009*a*, November). *Nature*, **462**(7269), 83–86.
Mattsson, Johan, Wyss, Hans M., Fernandez-Nieves, Alberto, Miyazaki, Kunimasa,

Hu, Zhibing, Reichman, David R., and Weitz, David A. (2009*b*, November). *Nature*, **462**(7269), 83–86.
Mayer, P., Bissig, H., Berthier, L., Cipelletti, L., Garrahan, J. P., Sollich, P., and Trappe, V. (2004, Sep). *Phys. Rev. Lett.*, **93**(11), 115701.
Mazoyer, S., Ebert, F., Maret, G., and Keim, P. (2009). *Europhys. Lett.*, **88**(6), 66004.
McKenna, Gregory B. (2003). *J. Phys.: Cond. Matt.*, **15**(11), S737–S763.
Meller, Amit and Stavans, Joel (1992, June). *Phys. Rev. Lett.*, **68**(24), 3646–3649.
Mohraz, Ali, Weeks, Eric R., and Lewis, Jennifer A. (2008). *Phys. Rev. E*, **77**(6), 060403(R).
Moller, P. C. F., Rodts, S., Michels, M. A. J., and Bonn, Daniel (2008). *Phys. Rev. E*, **77**(4), 041507.
Ngai, K. L. (1999, December). *J. Phys. Chem. B*, **103**(48), 10684–10694.
Ngai, K. L. and Rendell, R. W. (1998, February). *Phil. Mag. B*, **77**(2), 621–631.
Nugent, Carolyn R., Edmond, Kazem V., Patel, Hetal N., and Weeks, Eric R. (2007). *Phys. Rev. Lett.*, **99**(2), 025702.
O'Hern, Corey S., Silbert, Leonardo E., Liu, Andrea J., and Nagel, Sidney R. (2003, Jul). *Phys. Rev. E*, **68**(1), 011306.
O'Hern, Corey S., Silbert, Leonardo E., Liu, Andrea J., and Nagel, Sidney R. (2004, Oct). *Phys. Rev. E*, **70**(4), 043302.
Olmsted, P. (1999, April). *Current Opinion in Colloid & Interface Science*, **4**(2), 95–100.
Parisi, Giorgio and Zamponi, Francesco (2005). *J. Chem. Phys.*, **123**(14), 144501.
Perera, Donna N. and Harrowell, Peter (1999). *J. Chem. Phys.*, **111**(12), 5441–5454.
Pham, K. N., Puertas, A. M., Bergenholtz, J., Egelhaaf, S. U., Moussaid, A., Pusey, P. N., Schofield, A. B., Cates, M. E., Fuchs, M., and Poon, W. C. K. (2002, April). *Science*, **296**(5565), 104–106.
Phan, See-Eng, Russel, William B., Cheng, Zhengdong, Zhu, Jixiang, Chaikin, Paul M., Dunsmuir, John H., and Ottewill, Ronald H. (1996, Dec). *Phys. Rev. E*, **54**(6), 6633–6645.
Poon, W. C. K. (2002). *J. Phys.: Cond. Matt.*, **14**(33), R859–R880.
Poon, Wilson C. K., Meeker, S. P., Pusey, P. N., and Segrè, P. N. (1996, November). *Journal of Non-Newtonian Fluid Mechanics*, **67**, 179–189.
Puertas, Antonio M., Fuchs, Matthias, and Cates, Michael E. (2004). *J. Chem. Phys.*, **121**(6), 2813–2822.
Pusey, P. (1999, June). *Current Opinion in Colloid & Interface Science*, **4**(3), 177–185.
Pusey, P. N. (1978). *Journal of Physics A: Mathematical and General*, **11**(1), 119–135.
Pusey, Peter N. (1991), pp. 763–943. Les Houches session LI.
Pusey, P. N., Fijnaut, H. M., and Vrij, A. (1982). *J. Chem. Phys.*, **77**(9), 4270–4281.
Pusey, P. N. and van Megen, W. (1986, March). *Nature*, **320**(6060), 340–342.
Pusey, P. N. and van Megen, W. (1987, Nov). *Phys. Rev. Lett.*, **59**(18), 2083–2086.
Pusey, P. N., Zaccarelli, E., Valeriani, C., Sanz, E., Poon, Wilson C. K., and Cates, Michael E. (2009, December). *Phil. Trans. Roy. Soc. A*, **367**(1909), 4993–5011.

Richert, Ranko (2002). *J. Phys.: Cond. Matt.*, **14**(23), R703–R738.
Robert, A., Wandersman, E., Dubois, E., Dupuis, V., and Perzynski, R. (2006). *Europhys. Lett.*, **75**(5), 764–770.
Roovers, Jacques (1994, September). *Macromolecules*, **27**(19), 5359–5364.
Roth, Connie B. and Dutcher, John R. (2005, October). *Journal of Electroanalytical Chemistry*, **584**(1), 13–22.
Royall, C. P., Leunissen, M. E., and Blaaderen, A. Van (2003). *J. Phys.: Cond. Matt.*, **15**(48), S3581–S3596.
Russel, W. B., Saville, D. A., and Schowalter, W. R. (1992, March). *Colloidal Dispersions (Cambridge Monographs on Mechanics)*. Cambridge University Press.
Saltzman, Erica J. and Schweizer, Kenneth S. (2006*a*). *J. Chem. Phys.*, **125**(4), 044509.
Saltzman, Erica J. and Schweizer, Kenneth S. (2006*b*). *Phys. Rev. E*, **74**(6), 061501.
Schaertl, W. and Sillescu, H. (1994, December). *Journal of Statistical Physics*, **77**(5), 1007–1025.
Schall, Peter, Weitz, David A., and Spaepen, Frans (2007, December). *Science*, **318**(5858), 1895–1899.
Schätzel, Klaus (1991). *Journal of Modern Optics*, **38**(9), 1849–1865.
Schope, H. J., Bryant, G., and van Megen, W. (2007). *J. Chem. Phys.*, **127**, 084505.
Schweizer, Kenneth S. and Saltzman, Erica J. (2003). *J. Chem. Phys.*, **119**(2), 1181–1196.
Schweizer, K. S. and Saltzman, E. J. (2004, December). *The J. Phys. Chem. B*, **108**(51), 19729–19741.
Segrè, P. N., Behrend, O. P., and Pusey, P. N. (1995*a*, Nov). *Phys. Rev. E*, **52**(5), 5070–5083.
Segrè, P. N., Meeker, S. P., Pusey, P. N., and Poon, W. C. K. (1995*b*, Jul). *Phys. Rev. Lett.*, **75**(5), 958–961.
Segrè, P. N., Meeker, S. P., Pusey, P. N., and Poon, W. C. K. (1995*c*, Jul). *Phys. Rev. Lett.*, **75**(5), 958–961.
Segrè, P. N., Meeker, S. P., Pusey, P. N., and Poon, W. C. K. (1996, July). *Phys. Rev. Lett.*, **77**(3), 585.
Senff, H., Richtering, W., Norhausen, Ch, Weiss, A., and Ballauff, M. (1999, January). *Langmuir*, **15**(1), 102–106.
Sessoms, David A., Bischofberger, Irmgard, Cipelletti, Luca, and Trappe, Véronique (2009, December). *Phil. Trans. Roy. Soc. A*, **367**(1909), 5013–5032.
Sillescu, Hans (1999, February). *J. Non-Cryst. Solids*, **243**(2-3), 81–108.
Simeonova, Nikoleta B. and Kegel, Willem K. (2004, Jul). *Phys. Rev. Lett.*, **93**(3), 035701.
Speedy, Robin J. (1998). *Molecular Physics*, **95**(2), 169–178.
Stillinger, Frank H. (1995, March). *Science*, **267**(5206), 1935–1939.
Stober, W. (1968, January). *J. Colloid Interf. Sci.*, **26**(1), 62–69.
Sutherland, W. (1905). *Phil. Mag.*, **9**, 781–785.
Szamel, G. and Flenner, E. (2004, September). *Europhys. Lett.*, **67**(5), 779–785.
Tokuyama, Michio (2007, May). *Physica A*, **378**(2), 157–166.
Tokuyama, Michio and Oppenheim, Irwin (1994, Jul). *Phys. Rev. E*, **50**(1), R16–R19.

Tokuyama, Michio and Oppenheim, Irwin (1995, June). *Physica A*, **216**(1-2), 85–119.
Torquato, S., Truskett, T. M., and Debenedetti, P. G. (2000, Mar). *Phys. Rev. Lett.*, **84**(10), 2064–2067.
Trappe, V., Pitard, E., Ramos, L., Robert, A., Bissig, H., and Cipelletti, L. (2007, Nov). *Phys. Rev. E*, **76**(5), 051404.
Trappe, V. and Sandkuhler, P. (2004, April). *Current Opinion in Colloid & Interface Science*, **8**(6), 494–500.
Utter, Brian and Behringer, R. P. (2008). *Phys. Rev. Lett.*, **100**(20), 208302.
van Blaaderen, A. and Wiltzius, P. (1995, November). *Science*, **270**, 1177–1179.
van Megen, W., Mortensen, T. C., Williams, S. R., and Müller, J. (1998, November). *Phys. Rev. E*, **58**(5), 6073–6085.
van Megen, W. and Pusey, P. N. (1991, May). *Phys. Rev. A*, **43**(10), 5429–5441.
van Megen, W and Underwood, S. M. (1989). *J. Chem. Phys.*, **91**, 552–559.
van Megen, W. and Underwood, S. M. (1993, Jan). *Phys. Rev. E*, **47**(1), 248–261.
van Megen, W. and Underwood, S. M. (1994, May). *Phys. Rev. E*, **49**(5), 4206–4220.
van Megen, W. and Williams, Stephen R. (2010, Apr). *Phys. Rev. Lett.*, **104**(16), 169601.
Vermant, J. (2001, November). *Current Opinion in Colloid & Interface Science*, **6**(5-6), 489–495.
Vidal Russell, E. and Israeloff, N. E. (2000, December). *Nature*, **408**(6813), 695–698.
Vrij, A. (1976). *Pure and Applied Chemistry*, **48**(4), 471–483.
Wandersman, E., Duri, A., Robert, A., Dubois, E., Dupuis, V., and Perzynski, R. (2008). *J. Phys.: Cond. Matt.*, **20**(15), 155104.
Weeks, Eric R., Crocker, J. C., Levitt, Andrew C., Schofield, Andrew, and Weitz, D. A. (2000, January). *Science*, **287**(5453), 627–631.
Weeks, Eric R., Crocker, John C., and Weitz, D. A. (2007). *J. Phys.: Cond. Matt.*, **19**(20), 205131.
Weeks, Eric R. and Weitz, D. A. (2002, Aug). *Phys. Rev. Lett.*, **89**(9), 095704.
Weitz, D. A. and Pine, D. J. (1993). In *Dynamic Light scattering* (ed. W. Brown), pp. 652–720. Clarendon Press, Oxford.
Williams, S. R. and van Megen, W. (2001). *Phys. Rev. E*, **64**(4), 041502.
Wochner, Peter, Gutt, Christian, Autenrieth, Tina, Demmer, Thomas, Bugaev, Volodymyr, Ortiz, Alejandro D., Duri, Agnès, Zontone, Federico, Grübel, Gerhard, and Dosch, Helmut (2009, July). *Proc. Nat. Acad. Sci.*, **106**(28), 11511–11514.
Wong, Apollo P. Y. and Wiltzius, P. (1993). *Rev. Sci. Inst.*, **64**(9), 2547–2549.
Xu, Ning, Haxton, Thomas K., Liu, Andrea J., and Nagel, Sidney R. (2009, Dec). *Phys. Rev. Lett.*, **103**(24), 245701.
Yamamoto, R. and Onuki, A. (1997). *Europhysics Letters (EPL)*, **40**(1), 61–66.
Yamamoto, Ryoichi and Onuki, Akira (1998). *Phys. Rev. E*, **58**(3), 3515–3529.
Yethiraj, Anand and van Blaaderen, Alfons (2003, January). *Nature*, **421**(6922), 513–517.
Yunker, Peter, Zhang, Zexin, Aptowicz, Kevin, and Yodh, A. (2009, Sep). *Phys. Rev. Lett.*, **103**(11), 115701.
Zaccarelli, Emanuela (2007, August). *J. Phys.: Cond. Matt.*, **19**(32), 323101+.
Zaccarelli, E., Valeriani, C., Sanz, E., Poon, W. C. K., Cates, M. E., and Pusey, P. N.

(2009*a*, Sep). *Phys. Rev. Lett.*, **103**(13), 135704.

Zaccarelli, E., Valeriani, C., Sanz, E., Poon, W. C. K., Cates, M. E., and Pusey, P. N. (2009*b*, Sep). *Phys. Rev. Lett.*, **103**(13), 135704.

Zhu, Jixiang, Li, Min, Rogers, R., Meyer, W., Ottewill, R. H., Sts-73, Russel, W. B., and Chaikin, P. M. (1997, June). *Nature*, **387**(6636), 883–885.